SARS-CoV-2 T-cell epitopes define heterologous and COVID-19-induced T-cell recognition

Annika Nelde[1,2,3,#], Tatjana Bilich[1,2,3,#], Jonas S. Heitmann[1,3,#], Yacine Maringer[1,2,3], Helmut R. Salih[1,3,4], Malte Roerden[2,3,5], Maren Lübke[2], Jens Bauer[1,2], Jonas Rieth[1,2], Marcel Wacker[1,2], Andreas Peter[6], Sebastian Hörber[6], Bjoern Traenkle[7], Philipp D. Kaiser[7], Ulrich Rothbauer[7,8], Matthias Becker[7], Daniel Junker[7], Gérard Krause[9,10,11], Monika Strengert[9,10], Nicole Schneiderhan-Marra[7], Markus F. Templin[7], Thomas O. Joos[7], Daniel J. Kowalewski[12], Vlatka Stos-Zweifel[12], Michael Fehr[2], Michael Graf[13], Lena-Christin Gruber[1], David Rachfalski[1], Beate Preuß[5], Ilona Hagelstein[1,3], Melanie Märklin[1,3], Tamam Bakchoul[14], Cécile Gouttefangeas[2,3,4], Oliver Kohlbacher[13,15,16,17], Reinhild Klein[5], Stefan Stevanović[2,4], Hans-Georg Rammensee[2,3,4], Juliane S. Walz[1,2,3,5,*]

[1] Clinical Collaboration Unit Translational Immunology, German Cancer Consortium (DKTK), Department of Internal Medicine, University Hospital Tübingen, Tübingen, Germany

[2] Institute for Cell Biology, Department of Immunology, University of Tübingen, Tübingen, Germany

[3] Cluster of Excellence iFIT (EXC2180) "Image-Guided and Functionally Instructed Tumor Therapies", University of Tübingen, Tübingen, Germany

[4] German Cancer Consortium (DKTK) and German Cancer Research Center (DKFZ), partner site Tübingen, Tübingen, Germany

[5] Department of Hematology, Oncology, Clinical Immunology and Rheumatology, University Hospital Tübingen, Tübingen, Germany

[6] Institute for Clinical Chemistry and Pathobiochemistry, Department for Diagnostic Laboratory Medicine, University Hospital Tübingen, Tübingen, Germany

[7] NMI, Natural and Medical Sciences Institute at the University of Tübingen, Reutlingen, Germany

[8] Pharmaceutical Biotechnology, University of Tübingen, Tübingen, Germany

[9] Department of Epidemiology, Helmholtz Centre for Infection Research, Braunschweig, Germany

[10] TWINCORE GmbH, Centre for Experimental and Clinical Infection Research, a joint venture of the Hannover Medical School and the Helmholtz Centre for Infection Research, Hannover, Germany

[11] German Center for Infection Research, Braunschweig, Germany

[12] Immatics Biotechnologies GmbH, Tübingen, Germany

[13] Applied Bioinformatics, Center for Bioinformatics and Department of Computer Science, University of Tübingen, Tübingen, Germany

[14] Institute for Clinical and Experimental Transfusion Medicine, University Hospital Tübingen, Tübingen, Germany

[15] Institute for Bioinformatics and Medical Informatics, University of Tübingen, Germany

[16] Biomolecular Interactions, Max-Planck-Institute for Developmental Biology, Tübingen, Germany

[17] Institute for Translational Bioinformatics, University Hospital Tübingen, Tübingen, Germany

[#] These authors contributed equally to this work.

* Corresponding author:
PD Dr. med Juliane Sarah Walz
Otfried-Müller-Str. 10
72076 Tübingen
Germany
Phone: 0049 7071 2968746
Fax: 0049 7071 2925108
Mail: juliane.walz@med.uni-tuebingen.de

Summary paragraph

The SARS-CoV-2 pandemic calls for the rapid development of diagnostic, preventive, and therapeutic approaches. $CD4^+$ and $CD8^+$ T cell-mediated immunity is central for control of and protection from viral infections[1-3]. A prerequisite to characterize T-cell immunity, but also for the development of vaccines and immunotherapies, is the identification of the exact viral T-cell epitopes presented on human leukocyte antigens (HLA)[2-8]. This is the first work identifying and characterizing SARS-CoV-2-specific and cross-reactive HLA class I and HLA-DR T-cell epitopes in SARS-CoV-2 convalescents (n = 180) as well as unexposed individuals (n = 185) and confirming their relevance for immunity and COVID-19 disease course. SARS-CoV-2-specific T-cell epitopes enabled detection of post-infectious T-cell immunity, even in seronegative convalescents. Cross-reactive SARS-CoV-2 T-cell epitopes revealed preexisting T-cell responses in 81% of unexposed individuals, and validation of similarity to common cold human coronaviruses provided a functional basis for postulated heterologous immunity[9] in SARS-CoV-2 infection[10,11]. Intensity of T-cell responses and recognition rate of T-cell epitopes was significantly higher in the convalescent donors compared to unexposed individuals, suggesting that not only expansion, but also diversity spread of SARS-CoV-2 T-cell responses occur upon active infection. Whereas anti-SARS-CoV-2 antibody levels were associated with severity of symptoms in our SARS-CoV-2 donors, intensity of T-cell responses did not negatively affect COVID-19 severity. Rather, diversity of SARS-CoV-2 T-cell responses was increased in case of mild symptoms of COVID-19, providing evidence that development of immunity requires recognition of multiple SARS-CoV-2 epitopes. Together, the specific and cross-reactive SARS-CoV-2 T-cell epitopes identified in this work enable the identification of heterologous and post-infectious T-cell immunity and facilitate the development of diagnostic, preventive, and therapeutic measures for COVID-19.

Main

T cells control viral infections and provide immunological memory that enables long-lasting protection[1-3]. Whereas $CD4^+$ T helper cells orchestrate the immune response and enable B cells to produce antibodies, $CD8^+$ cytotoxic T cells eliminate virus-infected cells. For both, recognition of viral antigens in the form of short peptides presented on human leukocyte antigens (HLA) is fundamental. In consequence, characterization of such viral T-cell epitopes[4,5,8] is crucial for the understanding of immune defense mechanisms, but also a prerequisite for the development of vaccines and immunotherapies[2,6,7,12].

The SARS-CoV-2 coronavirus causes COVID-19, which has become a worldwide pandemic with dramatic socioeconomic consequences[13,14]. Available treatment options are limited, and despite intensive efforts a vaccine is so far not available. Knowledge obtained from the two other zoonotic coronaviruses SARS-CoV-1 and MERS-CoV indicates that coronavirus (CoV)-specific T-cell immunity is an important determinant for recovery and long-term protection[15-18]. This is even more important since studies on humoral immunity to SARS-CoV-1 provided evidence that antibody responses are short-lived and can even cause or aggravate virus-associated lung pathology[19,20]. With regard to SARS-CoV-2, two very recent studies[10,11] described $CD4^+$ and $CD8^+$ T-cell responses to viral peptide megapools in donors that had recovered from COVID-19 and individuals not exposed to SARS-CoV-2, the latter being indicative of potential T-cell cross-reactivity[9,21]. The exact viral epitopes that mediate these T-cell responses against SARS-CoV-2, however, were not identified in these studies, but are prerequisite (i) to delineate the role of post-infectious and heterologous T-cell immunity in COVID-19, (ii) for establishing diagnostic tools to identify SARS-CoV-2 immunity, and, most importantly, (iii) to define target structures for the development of SARS-CoV-2-specific vaccines and immunotherapies. In this study, we define SARS-CoV-2-

specific and cross-reactive $CD4^+$ and $CD8^+$ T-cell epitopes in a large collection of SARS-CoV-2 convalescents as well as non-exposed individuals and their relevance for immunity and the course of COVID-19 disease.

Results

Identification of SARS-CoV-2-derived HLA class I- and HLA-DR-binding peptides

A novel prediction and selection workflow, based on the integration of the algorithms SYFPEITHI and NetMHCpan, identified 1,739 and 1,591 auspicious SARS-CoV-2-derived HLA class I- and HLA-DR-binding peptides across all 10 viral open-reading frames (ORFs, Fig. 1a, Extended Data Fig. 1a, b). Predictions were performed for the 10 and 6 most common HLA class I (HLA-A*01:01, -A*02:01, -A*03:01, -A*11:01, -A*24:02, -B*07:02, -B*08:01, -B*15:01, -B*40:01, and -C*07:02) and HLA-DR (HLA-DRB1*01:01, -DRB1*03:01, -DRB1*04:01, -DRB1*07:01, -DRB1*11:01, and -DRB1*15:01) allotypes covering 91.7% and 70.6% of the world population with at least one allotype, respectively[22,23] (Extended Data Fig. 1c and 2a). To identify broadly applicable SARS-CoV-2-derived T-cell epitopes, we selected 100 SARS-CoV-2-derived HLA class I-binding peptides comprising 10 peptides per HLA class I allotype across all 10 viral ORFs for immunogenicity screening (range 3 - 20 peptides per ORF, mean 10, Fig. 1b, c, Extended Data Fig. 1d-m, Supplementary Table 1). In addition, 20 SARS-CoV-2-derived promiscuous HLA-DR-binding peptides across all ORFs from peptide clusters of various HLA-DR allotype restrictions representing 99 different peptide-allotype combinations were included (Fig. 1d, e, Extended Data Fig. 2b-k, Supplementary Tables 2 and 3). Of these HLA-DR-binding peptides, 14/20 (70%) contained embedded SARS-CoV-2-derived HLA class I-binding peptides for 7/10 HLA class I allotypes. The complete panel of 120 SARS-CoV-2-derived peptides comprised 10% of the total SARS-CoV-2 proteome (57%

and 12% of nucleocapsid and spike protein, respectively; Extended Data Fig. 2l) and showed an equally distributed origin of structural ORF proteins (61/120 (51%)) encompassing spike, envelope, membrane and nucleocapsid proteins as well as non-structural or accessory ORFs (59/120 (49%)). The broad HLA class I and HLA-DR allotype-restriction of the selected SARS-CoV-2-derived peptides allowed for a total coverage of at least one HLA allotype in 97.6% of the world population (Fig. 1f). Recurrent mutations of SARS-CoV-2[24,25] affected only a minority of selected SARS-CoV-2-derived peptides with 14/120 (12%) sequences (1.7% at anchor position) including reported mutation sites (Fig. 1g, Supplementary Tables 4 and 5).

Validation and characterization of SARS-CoV-2-derived CD8$^+$ and CD4$^+$ T-cell epitopes

IFNγ ELISPOT screening of SARS-CoV-2 convalescents (SARS, group 1, n = 116, Extended Data Table 1, Supplementary Table 6) and donors never exposed to SARS-CoV-2 (PRE, group A, n = 104, samples collected prior to SARS-CoV-2 pandemic, Extended Data Table 1, Supplementary Table 7) validated 29/100 (29%) SARS-CoV-2-derived HLA class I- (3/10 HLA-A*01, 2/10 HLA-A*02, 3/10 HLA-A*03, 2/10 HLA-A*11, 5/10 HLA-A*24, 2/10 HLA-B*07, 4/10 HLA-B*08, 0/10 HLA-B*15, 5/10 HLA-B*40, 3/10 HLA-C*07) and 20/20 (100%) HLA-DR-binding peptides as naturally occurring T-cell epitopes (Fig. 2a-f, Extended Data Tables 2 and 3, Supplementary Fig. 1 and 2, Supplementary Table 8). Flow cytometry revealed that T-cell responses directed against HLA class I-binding peptides were mainly driven by IFNγ$^+$CD8$^+$ T cells, whereas HLA-DR-binding peptides were recognized by multifunctional (IFNγ$^+$TNF$^+$CD107a$^+$) CD4$^+$ T cells and in single donors additionally by CD8$^+$ T cells (Fig. 2b, d). 12/29 (41%) and 11/20 (55%) SARS-CoV-2-derived CD8$^+$ and CD4$^+$ T-cell epitopes were dominant epitopes (recognized by ≥ 50% of SARS donors) with recognition frequencies up to 83% (A01_P01) and 95% (DR_P16), respectively (Fig. 2e, f, Extended Data Tables 2 and 3). T-cell responses showed high inter-individual as well as inter-peptide intensity variation

(Supplementary Fig. 3). Overall, the intensity of HLA-DR-specific T-cell responses in the SARS group was significantly more pronounced compared to those directed against HLA class I T-cell epitopes (median 414 versus 56 calculated spot counts, Fig. 2g). All SARS-CoV-2-derived HLA-DR-binding peptides were found to be immunogenic, independently of the source ORF. SARS-CoV-2-derived HLA class I T-cell epitopes showed an equally distributed origin from structural (13/29 (45%)) and non-structural or accessory (16/29 (55%)) ORFs (Extended Data Table 2). However, ORF-specific differences regarding the proportion of validated HLA class I T-cell epitopes were observed, revealing the highest frequencies for ORF9 (50%, nucleocapsid protein), ORF1 (45%), and ORF3 (38%, Fig. 2h). The highest recognition rate in SARS donors was observed for HLA class I T-cell epitopes derived from ORF2 (55%, spike protein), ORF5 (52%, membrane protein), and ORF3 (45%), as well as for HLA-DR T-cell epitopes derived from ORF5 (95%, membrane protein), ORF8 (68%), and ORF4 (55%, envelope protein, Fig. 2i).

Cross-reactive T-cell responses to SARS-CoV-2-derived HLA class I and HLA-DR T-cell epitopes in unexposed individuals

Upon screening PRE group A, cross-reactive T-cell responses to 9/29 (31%) of the validated HLA class I and to 14/20 (70%) HLA-DR T-cell epitopes were detected. Recognition frequencies of single SARS-CoV-2 HLA class I and HLA-DR T-cell epitopes in PRE donors were lower compared to that of SARS group 1 (up to 27% for B08_P05 and 44% for DR_P01, Fig. 2e, f, Extended Data Tables 2 and 3). Recognition frequencies of HLA class I and HLA-DR T-cell epitopes in individual donors differed profoundly between the PRE and the SARS group within the different ORFs. ORF1-derived HLA class I (9%) and ORF8-derived HLA-DR (25%) T-cell epitopes showed the highest recognition frequencies in the PRE group, whereas none of the T-cell epitopes from ORF5 (membrane protein) and ORF10 that were frequently

recognized in SARS donors were detected by T cells in PRE donors (Fig. 2i). In line with the lower recognition frequencies of single SARS-CoV-2 T-cell epitopes (Fig. 2e, f), donor-specific recognition rates of HLA class I and HLA-DR SARS-CoV-2 T-cell epitopes were significantly lower in the PRE group (HLA class I, mean 26 $\pm$ 9; HLA-DR, mean 10 $\pm$ 5) than in the SARS group (HLA class I, mean 52 $\pm$ 23; HLA-DR, mean 52 $\pm$ 23, Fig. 3a). Alignments of the SARS-CoV-2 T-cell epitopes recognized by unexposed individuals revealed similarities to the four seasonal common cold human coronaviruses (HCoV-OC43, HCoV-229E, HCoV-NL63, HCoV-HKU1) with regard to amino acid sequences, physiochemical and/or HLA-binding properties for 14/20 (70%) of the epitopes, thereby providing clear evidence for SARS-CoV-2 T-cell cross-reactivity (Fig. 3b, Supplementary Tables 9 and 10, Supplementary Data 1).

Frequency of SARS-CoV-2 T-cell responses in COVID-19 convalescents and unexposed individuals

Epitope screening in SARS and PRE donors enabled the identification of SARS-CoV-2-specific T-cell epitopes recognized exclusively in convalescents after SARS-CoV-2 infection and of cross-reactive T-cell epitopes recognized by both, convalescents and SARS-CoV-2 unexposed individuals (Fig. 2e, f). To allow for standardized evaluation and determination of T-cell response frequencies to SARS-CoV-2, we designed broadly applicable HLA class I and HLA-DR SARS-CoV-2-specific and cross-reactive T-cell epitope compositions (EC, Fig. 3c, Extended Data Table 4). These EC were utilized for IFNγ ELISPOT assays in groups of convalescents (SARS group 2, n = 86, Extended Data Table 1, Supplementary Table 6) and unexposed donors (PRE group B, n = 94, Extended Data Table 1, Supplementary Table 7). Of the SARS donors, 100% showed T-cell responses to cross-reactive and/or specific EC (Fig. 3d, e), whereas 81% of PRE donors showed HLA class I (16%) and/or HLA-DR (77%) T-cell responses to cross-reactive EC (Fig. 3d). In line with the findings obtained with the screening group

(SARS group 1), the intensity of HLA class I T-cell responses was significantly lower compared to HLA-DR T-cell responses, both for specific (median calculated spot count HLA class I 379, HLA-DR 760) and cross-reactive EC (median calculated spot count HLA class I 86, HLA-DR 846, Fig. 3f, g). In line with the differences in recognition rates observed between SARS group 1 and PRE group A, the intensity of T-cell responses to cross-reactive EC was significantly lower in the PRE group (median calculated spot count HLA class I 14, HLA-DR 346) compared to the SARS group (Fig. 3g).

Relationship of SARS-CoV-2 T-cell and antibody responses

Anti-SARS-CoV-2 IgG antibody responses in SARS donors were analyzed in two independent assays. The S1 IgG ELISA assay revealed 149/178 (84%), 7/178 (4%), and 22/178 (12%) donors with positive, borderline, and no anti S1 antibody response, respectively (Fig. 4a). Of the borderline/none responders, 18/29 (62%) were also negative in a second, independent anti-nucleocapsid immunoassay (Fig. 4b). However, SARS-CoV-2-specific $CD8^+$ and/or $CD4^+$ T-cell responses were detected in 10/18 (56%) of these "antibody double-negative" donors (Fig. 4c). The intensity of SARS-CoV-2-specific and cross-reactive HLA-DR T-cell responses correlated with antibody levels (Fig. 4d, e), whereas no correlation was observed with HLA class I T-cell responses (Extended Data Fig. 3a, b). No correlation between antibody titers directed against the nucleocapsid of human common cold coronaviruses (HCoV-229E, HCoV-NL63, HCoV-OC43), as determined by bead-based serological multiplex assays and the intensity of cross-reactive $CD4^+$ and $CD8^+$ T-cell responses in the SARS group, was detected (Extended Data Fig. 3c-h).

Association of SARS-CoV-2-directed antibody and T-cell responses with clinical characteristics in COVID-19

Finally, the association of anti-SARS-CoV-2 antibody and T-cell responses with disease severity as assessed by a combinatorial symptom score (SC) of objective (fever ≥ 38.0°C) and patient-subjective disease symptoms was determined (Extended Data Table 1). Alike in critically ill patients[26], independently of age high antibody ratios significantly associated with disease severity in our collection of convalescent SARS donors (n = 180), which in general were in good health condition and had not been hospitalized (Fig. 4f, Extended Data Fig. 4a). Neither the intensity of SARS-CoV-2-specific nor of cross-reactive T-cell responses to HLA class I or HLA-DR EC correlated with disease severity (Fig. 4g). Rather, diversity of T-cell responses in terms of recognition rate of SARS-CoV-2 T-cell epitopes was decreased in patients with more severe COVID-19 symptoms (Fig. 4h, Extended Data Fig. 4b), providing evidence that development of protective immunity requires recognition of multiple SARS-CoV-2 epitopes.

Discussion

This study reports the first characterization of broadly applicable SARS-CoV-2-specific and cross-reactive T-cell epitopes of various HLA allotype restrictions across all viral ORFs identified in two large collections of donors recovered from SARS-CoV-2 infection as well as unexposed individuals. Our findings aid SARS-CoV-2 research with regard to the understanding of SARS-CoV-2 post-infectious and heterologous T-cell responses, but also regarding the development of prophylactic and therapeutic measures.

Cross-reactivity of T cells for different virus species or even amongst different pathogens is a well-known phenomenon[27,28] postulated to enable heterologous immunity to a pathogen after exposure to a non-identical pathogen[9,21,29]. Using predicted or random

SARS-CoV-2--derived peptide pools, two very recent studies reported preexisting SARS-CoV-2-directed T-cell responses in small groups of unexposed as well as SARS-CoV-2 seronegative individuals, thereby suggesting cross-reactivity between human common cold coronaviruses and SARS-CoV-2[10,11]. In our study we identified and characterized the exact T-cell epitopes that govern SARS-CoV-2 cross-reactivity and proved similarity to human common cold coronaviruses regarding individual peptide sequences, physiochemical and HLA-binding properties[30,31]. Notably, we detected SARS-CoV-2 cross-reactive T cells in 81% of unexposed individuals. To determine if these T-cells indeed mediate heterologous immunity and whether this explains the relatively small proportion of severely ill or, even in general, infected patients during this pandemic[32,33], a dedicated study using *e.g.* a matched case control, or retrospective cohort design applying our cross-reactive SARS-CoV-2 T-cell epitopes would be required. Our observation that intensity of T-cell responses and recognition rate of T-cell epitopes was significantly higher in convalescents compared to unexposed individuals suggests that not only expansion, but also a spread of SARS-CoV-2 T-cell response diversity occurs upon active infection.

At present, determination of immunity to SARS-CoV-2 relies on the detection of SARS-CoV-2 antibody responses. However, despite the high sensitivity reported for several assays there is still a substantial percentage of patients with negative or borderline antibody responses and thus unclear immunity status after SARS-CoV-2 infection[34]. Our SARS-CoV-2-specific T-cell epitopes, which are not recognized by T cells of unexposed donors, allowed for detection of specific T-cell responses even in donors without antibody responses, thereby providing evidence for T-cell immunity upon infection.

In line with previous data on acute and chronic viral infection[35,36], our data indicate an important role of SARS-CoV-2 $CD4^+$ T-cell responses in the natural course of infection, with the identification of multiple dominant HLA class-DR T-cell epitopes that elicit more frequent and intense immune response in SARS donors compared to the HLA class I T-cell epitopes. This guides selection of T-cell epitopes for vaccine design, also in light of the dependency of protective antibody responses on $CD4^+$ T cell help.

The pathophysiological involvement of the immune response in the course of COVID-19 is a matter of intense debate. Our finding that also in mainly non-hospitalized patients with a mild disease course high level antibody responses are associated with more severe symptoms of COVID-19 is in line with recent data on the correlation of antibody titers with disease severity in hospitalized patients[26]. Our data provide the first evidence that, on the contrary, the intensity of T-cell responses does not correlate with disease severity. This is of high relevance for the design of vaccines, as it provides evidence that disease aggravating effects might not hamper the development of prophylactic and therapeutic vaccination approaches aiming to induce SARS-CoV-2-specific T-cell responses. In contrast to the intensity of the T-cell response, recognition rates of SARS-CoV-2 T-cell epitopes by individual donors were lower in individuals with more severe COVID-19 symptoms. This observation, together with our data on increased T-cell epitope recognition rates after SARS-CoV-2 infection compared to preexisting T-cell responses in unexposed individuals and reports from other active or chronic viral infections associating diversity of T-cell response with anti-viral defense[37-39], provide evidence that natural development and vaccine-based induction of immunity to SARS-CoV-2 requires recognition of multiple SARS-CoV-2 epitopes. Confirmation of this observation in a larger SARS cohort including hospitalized patients is warranted and requires single epitope-based methods to determine T-cell epitope recognition rates as

enabled by our SARS-CoV-2 T-cell epitopes. Moreover, our data underline the high importance of the identified T-cell epitopes for further studies of SARS-CoV-2 immunity, but also for the development of preventive and therapeutic COVID-19 measures. Using the SARS-CoV-2 T-cell epitopes we are currently preparing two clinical first-in-man studies (EudraCT 2020-002502-75; EudraCT 2020-002519-23) to evaluate a multi-peptide vaccine for induction of broad T-cell immunity to SARS-CoV-2 to combat COVID-19.

Methods

Patients and blood samples

Blood and serum samples as well as questionnaire-based assessment of donor characteristics and disease symptoms from convalescent volunteers after SARS-CoV-2 infection were collected at the University Hospital Tübingen, Germany from 4/2020 - 5/2020 (SARS collection n = 180). SARS-CoV-2 infection was confirmed by PCR test after nasopharyngeal swab. SARS donor recruitment was performed by online and paper-based calls. Sample collection for each SARS donor was performed approximately three to eight weeks after the end of symptoms and/or negative virus smear. Peripheral blood mononuclear cells (PBMCs) asserted from blood donations of healthy individuals prior to the SARS-CoV-2 pandemic (06/2007 - 11/2019) at the Department of Immunology, University of Tübingen were used to assess preexisting SARS-CoV-2 T-cell responses (PRE collection, n = 185). Informed consent was obtained in accordance with the Declaration of Helsinki protocol. The study was approved by and performed according to the guidelines of the local ethics committees (179/2020/BO2). PBMCs were isolated by density gradient centrifugation and stored at -80°C until further use. Serum was separated by centrifugation for 10 min and the supernatant was stored at -80°C. HLA typing was carried out by Immatics Biotechnology GmbH and the Department of Hematology and Oncology at the University Hospital Tübingen. Symptom score (SC) was determined by combining objective (fever ≥ 38.0°C) and subjective disease symptoms of individual donors. SARS and PRE collections were split into two groups for T-cell epitope screening and standardized immunity evaluation. Detailed SARS and PRE donor characteristics as well as information on allocation of the donors to the experimental groups are provided in Extended Data Table 1 and Supplementary Tables 6 and 7.

Data retrieval

The complete highly conserved and representative annotated proteome sequence of SARS-CoV-2 isolate Wuhan-Hu-1 containing ten different open-reading frames (ORFs) was retrieved from the NCBI database with the accession number MN908947[40]. The amino acid sequence is identical to the reference sequence (EPI_ISL_412026) defined by Wang *et al.* conducting multiple sequence alignments and phylogenetic analyses of 95 full-length genomic sequences[24].

Prediction of SARS-CoV-2-derived HLA class I-binding peptides

The protein sequences of all ten ORFs were split into 9 - 12 amino acid long peptides covering the complete proteome of the virus. The prediction algorithms NetMHCpan 4.0[41-43] and SYFPEITHI 1.0[44] were used to predict the binding of peptides to HLA-A*01:01, -A*02:01, -A*03:01, -A*11:01, -A*24:02, -B*07:02, -B*08:01, -B*15:01, -B*40:01, and -C*07:02. Only peptides predicted as HLA-binding peptides by both algorithms (SYFPEITHI score ≥ 60%, NetMHCpan rank ≤ 2) for the respective allotype were further examined. Peptides containing cysteines were excluded to avoid dimerization in a potential subsequent vaccine production process. Peptides derived from the ORF1 polyprotein spanning the cleavage sites of the comprised different protein chains were excluded. An averaged rank combining NetMHCpan- and SYFPEITHI-derived prediction scores was calculated and peptides were ranked for each allotype and ORF separately. Through rank-based selection one peptide for each ORF and each allotype, respectively was selected. For peptides with equal averaged ranks, peptides with higher SYFPEITHI scores were nominated. For some HLA allotypes not every ORF gave rise to an appropriate HLA-binding peptide. To receive 10 peptides per HLA allotype and ORF, remaining slots were filled with additional peptides from the ORF9 nucleocapsid protein, the ORF2 spike protein, and ORF1.

Prediction of SARS-CoV-2-derived HLA-DR-binding peptides

For HLA-DR predictions all ten ORFs were split into peptides of 15 amino acids, resulting in a total of 9,561 peptides. The prediction algorithm SYFPEITHI 1.0 was used to predict the binding to HLA-DRB1*01:01, -DRB1*03:01, -DRB1*04:01, -DRB1*07:01, -DRB1*11:01, and -DRB1*15:01. The 5% (2% for ORF1) top-scoring peptides of each ORF (based on the total length of each ORF) and each HLA-DR allotype were selected. Position-based sorting of peptides within each ORF revealed peptide clusters of promiscuous peptides binding to several HLA-DR allotypes. Through cluster-based selection, peptide clusters of promiscuous peptides with a common core sequence of 9 amino acids were selected. Thereby, 10 and 2 clusters were selected for the ORF9 nucleocapsid and the ORF2 spike protein as well as one cluster for each of the remaining ORFs. Of each selected cluster one representative peptide was selected for immunogenicity analysis excluding cysteine containing peptides.

Sequence and physiochemical property alignments to common cold human coronaviruses

Sequence and physiochemical property alignments of the SARS-CoV-2-derived peptide sequences with the four seasonal common cold human coronaviruses (HCoV-OC43, HCoV-229E, HCoV-NL63, HCoV-HKU1) were performed by NCBI BLAST[45,46] and PepCalc (https://pepcalc.com/).

IFNγ ELISPOT assay following 12-day *in vitro* stimulation

Synthetic peptides were provided by EMC Microcollections GmbH and INTAVIS Bioanalytical Instruments AG. PBMCs were pulsed with HLA class I or HLA-DR peptide pools (1 µg/mL per peptide for class I or 5 µg/mL for HLA-DR) and cultured for 12 days adding 20 U/mL IL-2 (Novartis) on days 3, 5, and 7. Peptide-stimulated PBMCs were analyzed by enzyme-linked immunospot (ELISPOT) assay in duplicates (if not mentioned otherwise). 200.000 - 800.000

cells per well were incubated with 1 µg/mL (class I) or 2.5 µg/mL (HLA-DR) of single peptides in 96-well plates coated with anti-IFNγ antibody (clone 1-D1K, 2 µg/mL, MabTech). PHA (Sigma-Aldrich) served as positive control. After 22 - 24 h incubation, spots were revealed with anti-IFNγ biotinylated detection antibody (clone 7-B6-1, 0.3 µg/mL, MabTech), Extraavidin−Alkaline Phosphatase (1:1,000 dilution, Sigma-Aldrich) and BCIP/NBT (5-bromo-4-chloro-3-indolyl-phosphate/nitro-blue tetrazolium chloride, Sigma-Aldrich). Spots were counted using an ImmunoSpot S5 analyzer (CTL) and T-cell responses were considered positive when mean spot count was at least three-fold higher than the mean spot count of the negative control. Calculated spot counts indicate the mean spot count of duplicates normalized to 5 x 10^5 cells minus the normalized mean spot count of the respective negative control. For negative control peptides see Supplementary Table 11. For HLA-C*07-restricted peptides, screening in PRE donors was performed using samples of HLA-B*07^+ samples due to unavailable HLA-C typing and the known linkage disequilibrium of HLA-B*07 and -C*07[47,48].

Intracellular cytokine and cell surface marker staining

Peptide-specific T cells were further characterized by intracellular cytokine and cell surface marker staining. PBMCs were incubated with 10 µg/mL of peptide, 10µg/mL Brefeldin A (Sigma-Aldrich), and a 1:500 dilution of GolgiStop (BD) for 12 - 16 h. Staining was performed using Cytofix/Cytoperm solution (BD), APC/Cy7 anti-human CD4 (BD), PE/Cy7 anti-human CD8 (Beckman Coulter), Pacific Blue anti-human TNF, FITC anti-human CD107a, and PE anti-human IFNγ monoclonal antibodies (BioLegend). PMA (5 µg/ml) and ionomycin (1 µM, Sigma-Aldrich) served as positive control. Viable cells were determined using Aqua live/dead (Invitrogen). All samples were analyzed on a FACS Canto II cytometer (BD) and evaluated using FlowJo software version 10.0.7 (BD).

SARS-CoV-2 IgG ELISA (EUROIMMUN)

The 96-well SARS-CoV-2 IgG ELISA assay (EUROIMMUN) was performed on an automated BEP 2000 Advance® system (Siemens Healthcare Diagnostics GmbH) according to the manufacturer's instructions. The ELISA assay detects anti-SARS-CoV-2 IgG directed against the S1 domain of the viral spike protein and relies on an assay-specific calibrator to report a ratio of specimen absorbance to calibrator absorbance. The final interpretation of positivity is determined by ratio above a threshold value given by the manufacturer: positive (ratio ≥ 1.1), borderline (ratio 0.8 - 1.0) or negative (ratio < 0.8). Quality control was performed following the manufacturer's instructions on each day of testing.

Elecsys® anti-SARS-CoV-2 immunoassay (Roche Diagnostics GmbH)

The Elecsys® anti-SARS-CoV-2 assay is an ECLIA (electrogenerated chemiluminescence immunoassay) assay designed by Roche Diagnostics GmbH and was used according to manufacturer's instructions. It is intended for the detection of high affinity antibodies (including IgG) directed against the nucleocapsid protein of SARS-CoV-2 in human serum. Readout was performed on the Cobas ae411 analyzer. Negative results were defined by a cut-off index (COI) of < 1.0. Quality control was performed following the manufacturer's instructions on each day of testing.

Generation of expression constructs for the production of viral antigens

The cDNAs encoding the nucleocapsid proteins of HCoV-OC43, HCoV-NL63, and HCoV-229E (gene bank accession numbers YP_009555245.1; YP_003771.1; NP_073556.1) were produced with a N-terminal hexahistidine (His_6)-tag by gene synthesis (ThermoFisher Scientific) and cloned using standard techniques into NdeI/HindIII sites of the bacterial expression vector pRSET2b (ThermoFisher Scientific).

Protein expression and purification

To express the viral nucleocapsid proteins the respective expression constructs were transformed in *E.coli* BL21(DE3) cells. Protein expression was induced in 1 L TB medium at an optical density (OD_{600} of 2.5 - 3) by addition of 0.2 mM isopropyl-β-D-thiogalactopyranoside (IPTG) for 16 h at 20°C. Cells were harvested by centrifugation (10 min, 6000 x g) and the pellets were suspended in binding buffer (1x PBS, 0.5 M NaCl, 50 mM imidazole, 2 mM PMSF, 2 mM $MgCl_2$, 150 µg/mL lysozyme (Merck) and 625 µg/mL DNAse I (Applichem)). The cell suspensions were sonified for 15 min (Bandelin Sonopuls HD70 - power MS72/D, cycle 50%) on ice, incubated for 1 h at 4°C in a rotary shaker and sonified again. After centrifugation (30 min at 20,000 x g) urea was added to a final concentration of 6 M to the soluble protein extract. The extract was filtered through a 0.45 µm filter and loaded on a pre-equilibrated 1-ml HisTrap^{FF} column (GE Healthcare). The bound His-tagged nucleocapsid proteins were eluted by a linear gradient (30 mL) ranging from 50 to 500 mM imidazole in elution buffer (1x PBS, pH 7.4, 0.5 M NaCl, 6 M Urea). Elution fractions (0.5 mL) containing the His-tagged nucleocapsid proteins were pooled and dialyzed (D-Tube Dialyzer Mega, Novagen) into PBS. All purified proteins were analyzed via standard SDS-PAGE followed by staining with InstantBlue (Expedeon) and immunoblotting using an anti-His antibody (Penta-His Antibody, #34660, Qiagen) in combination with a donkey-anti-mouse antibody labeled with AlexaFluor647 (Invitrogen) on a Typhoon Trio (GE Healthcare, excitation 633 nM, emission filter settings 670 nM BP 30) to confirm protein integrity.

Preparation of beads for the serological multiplex assay

Antigens were covalently immobilized on spectrally distinct populations of carboxylated paramagnetic beads (MagPlex Microspheres, Luminex Corporation, Austin, TX) using 1-Ethyl-3-(3-dimethylaminopropyl) carbodiimide (EDC) / sulfo-N-hydroxysuccinimide (sNHS)

chemistry. For immobilization, a magnetic particle processor (KingFisher 96, ThermoFischer Scientific) was used. Bead stocks were vortexed thoroughly and sonificated for 15 seconds. A 96-deep-well plate and tip comb was blocked with 1.1 mL 0.5% (v/v) Triton X-100 for 10 minutes. Afterwards, 83 µL of 0.065% (v/v) Triton X-100 and 1 mL bead stock were added to each well. Finally, each well contained 0.005% (v/v) Triton X-100 and 12.5 x 10^7 beads of one single bead population. The beads were washed twice with 500 µL activation buffer (100 mM Na_2HPO_4, pH 6.2, 0.005% (v/v) Triton X-100) and beads were activated for 20 min in 300 µL activation mix containing 5 mg/mL EDC and 5 mg/mL sNHS in activation buffer. Following activation, the beads were washed twice with 500 µL coupling buffer (500 mM MES, pH 5.0 + 0.005% (v/v) Triton X-100). Antigens were diluted to 39 µg/mL in coupling buffer and incubated with the activated beads for 2 h at 21°C to immobilize the antigens on the surface. Antigen-coupled beads were washed twice with 800 µL wash buffer (1x PBS + 0.005% (v/v) Triton X-100) and were finally resuspended in 1 mL storage buffer (1x PBS + 1% (w/v) BSA + 0.05% (v/v) ProClin). The beads were stored at 4°C until further use.

Bead-based serological multiplex assay

To detect human IgG directed against nucleocapsid proteins from three different coronavirus species (HCoV-229E, HCoV-NL63, HCoV-OC43), a bead-based multiplex assay was performed. All antigens were immobilized on different bead populations as described above. The individual bead populations were combined to a bead mix. 25 µL of diluted serum sample were added to 25 µL of the bead mix resulting in a final sample dilution of 1:400 and incubated for 2 h at 21°C. Unbound antibodies were removed by washing the beads three times with 100 µL wash buffer (1x PBS + 0.05% (v/v) Tween20) per well using a microplate washer (Biotek 405TS, Biotek Instruments GmbH). Bound antibodies were detected by incubating the beads with PE-labeled goat-anti-human IgG detection antibodies

for 45 min at 21°C. Measurements were performed using a Luminex FlexMap 3D instrument using Luminex xPONENT Software (sample size: 80 µL, 100 events; gate: 7,500 - 15,000; reporter gain: Standard PMT). Data analysis was performed on Mean Fluorescence Intensity (MFI).

Software and statistical analysis

The population coverage of HLA allotypes was calculated by the IEDB population coverage tool (www.iedb.org). Flow cytometric data was analyzed using FlowJo 10.0.8 (Treestar). Data are displayed as mean with standard deviation, box plot as median with 25% or 75% quantiles and min/max whiskers. Continuous data were tested for distribution and individual groups were tested by use of unpaired students-t test, Mann-Whitney-U test or Kruskal-Wallis-test and corrected for multiple comparison as indicated. Spearman rho (ρ) was calculated for correlation between continuous data. A logistic regression model was used to calculate odds ratios and 95% confidence interval (CI). Factors before the outcome and measured continuous variables were included in the model. Missing data were included in tables and in descriptive analysis. Graphs were plotted using GraphPad Prism 8.4.0. Statistical analyses were conducted using GraphPad Prism 8.4.0 and JMP® Pro (SAS Institute Inc., version 14.2) software. *P* values of < 0.05 were considered statistically significant.

Acknowledgements

We thank all SARS and PRE donors for their support of our research. We thank Ulrike Schmidt, Christine Bauer, Antje Petz, Martina Storz, Isolde Riedlinger, Sabrina Sauter, Sabrina Augstein, Celine Reiß, Valentina Agrusa, Santhana Dethling, Michael Beller and Claudia Falkenburger for technical support and project coordination. This work was supported by the Bundesministerium für Bildung und Forschung (BMBF, FKZ:01KI20130), the Deutsche Forschungsgemeinschaft (DFG, German Research Foundation, Grant WA 4608/1-2), the Deutsche Forschungsgemeinschaft under Germany's Excellence Strategy (Grant EXC2180-390900677), the German Cancer Consortium (DKTK), the Wilhelm Sander Stiftung (Grant 2016.177.2), the José Carreras Leukämie-Stiftung (Grant DJCLS 05 R/2017), and the Fortüne Program of the University of Tübingen (Fortüne number 2451-0-0 and 2581-0-0). Multiplex antibody detection against common cold coronaviruses is part of a project that has received funding from the European Union's Horizon 2020 research and innovation program under grant agreement No 101003480 - CORESMA.

Authorship Contributions

A.N., H.-G.R., S.S., C.G., J.S.W. designed the study; A.N., S.S., and J.S.W. performed *in silico* prediction and selection of candidate peptides; T.Bi., Y.M., M.L, J.B., J.R., M.W., M.F., I.H., M.M. conducted *in vitro* T-cell experiments; B.P., R.K., D.J.K. and V.S-Z. conducted HLA allotype analysis; B.T., P.D.K., and U.R. generated expression plasmids, purified proteins for multiplex serological Luminex assay which was developed and conducted by M.B., D.J., G.K., M.S., N.S-M., M.F.T., T.O.J; SARS-CoV-2 IgG were detected by S.H., A.P.; J.S.H., M.R., T.Ba., L.-C.G., D.R., H.R.S., J.S.W. conducted patient data and sample collection as well as medical evaluation and analysis; A.N., T.Bi., J.S.H., M.G., O.K., J.S.W. analyzed data and performed

statistical analyses; A.N., T.Bi., J.S.H., H.R.S., J.S.W. drafted the manuscript; H.-G.R., S.S., J.S.W. supervised the study.

Data availability statement

All data that support the findings of this study are provided with the manuscript. Further source data are available from the corresponding author upon request.

Disclosure of Conflicts of Interest

Daniel Kowalewski and Vlatka Stos-Zweifel are employees of the Immatics Biotechnologies GmbH. Hans-Georg Rammensee is shareholder of Immatics Biotechnologies GmbH and Curevac AG. The other authors declare no competing financial interests.

References

1 Swain, S. L., McKinstry, K. K. & Strutt, T. M. Expanding roles for CD4(+) T cells in immunity to viruses. *Nat Rev Immunol* **12**, 136-148, doi:10.1038/nri3152 (2012).
2 Rosendahl Huber, S., van Beek, J., de Jonge, J., Luytjes, W. & van Baarle, D. T cell responses to viral infections - opportunities for Peptide vaccination. *Front Immunol* **5**, 171, doi:10.3389/fimmu.2014.00171 (2014).
3 Seder, R. A., Darrah, P. A. & Roederer, M. T-cell quality in memory and protection: implications for vaccine design. *Nat Rev Immunol* **8**, 247-258, doi:10.1038/nri2274 (2008).
4 Khan, N. *et al.* T cell recognition patterns of immunodominant cytomegalovirus antigens in primary and persistent infection. *J Immunol* **178**, 4455-4465, doi:10.4049/jimmunol.178.7.4455 (2007).
5 Falk, K. *et al.* Analysis of a naturally occurring HLA class I-restricted viral epitope. *Immunology* **82**, 337-342 (1994).
6 Einsele, H. *et al.* Infusion of cytomegalovirus (CMV)-specific T cells for the treatment of CMV infection not responding to antiviral chemotherapy. *Blood* **99**, 3916-3922, doi:10.1182/blood.v99.11.3916 (2002).
7 Tan, A. C. *et al.* The design and proof of concept for a CD8(+) T cell-based vaccine inducing cross-subtype protection against influenza A virus. *Immunol Cell Biol* **91**, 96-104, doi:10.1038/icb.2012.54 (2013).
8 Lubke, M. *et al.* Identification of HCMV-derived T cell epitopes in seropositive individuals through viral deletion models. *J Exp Med* **217**, doi:10.1084/jem.20191164 (2020).
9 Petrova, G., Ferrante, A. & Gorski, J. Cross-reactivity of T cells and its role in the immune system. *Crit Rev Immunol* **32**, 349-372, doi:10.1615/critrevimmunol.v32.i4.50 (2012).
10 Grifoni, A. *et al.* Targets of T Cell Responses to SARS-CoV-2 Coronavirus in Humans with COVID-19 Disease and Unexposed Individuals. *Cell*, doi:10.1016/j.cell.2020.05.015 (2020).
11 Braun, J. *et al.* Presence of SARS-CoV-2 reactive T cells in COVID-19 patients and healthy donors. *medRxiv*, 2020.2004.2017.20061440, doi:10.1101/2020.04.17.20061440 (2020).
12 Mudd, P. A. *et al.* Vaccine-induced CD8+ T cells control AIDS virus replication. *Nature* **491**, 129-133, doi:10.1038/nature11443 (2012).
13 Mo, P. *et al.* Clinical characteristics of refractory COVID-19 pneumonia in Wuhan, China. *Clin Infect Dis*, doi:10.1093/cid/ciaa270 (2020).
14 Khan, S. *et al.* The emergence of a novel coronavirus (SARS-CoV-2), their biology and therapeutic options. *J Clin Microbiol*, doi:10.1128/JCM.00187-20 (2020).
15 Zhao, J. *et al.* Airway Memory CD4(+) T Cells Mediate Protective Immunity against Emerging Respiratory Coronaviruses. *Immunity* **44**, 1379-1391, doi:10.1016/j.immuni.2016.05.006 (2016).
16 Zhao, J., Zhao, J. & Perlman, S. T cell responses are required for protection from clinical disease and for virus clearance in severe acute respiratory syndrome coronavirus-infected mice. *J Virol* **84**, 9318-9325, doi:10.1128/JVI.01049-10 (2010).

17 Channappanavar, R., Fett, C., Zhao, J., Meyerholz, D. K. & Perlman, S. Virus-specific memory CD8 T cells provide substantial protection from lethal severe acute respiratory syndrome coronavirus infection. *J Virol* **88**, 11034-11044, doi:10.1128/JVI.01505-14 (2014).
18 Ng, O. W. *et al.* Memory T cell responses targeting the SARS coronavirus persist up to 11 years post-infection. *Vaccine* **34**, 2008-2014, doi:10.1016/j.vaccine.2016.02.063 (2016).
19 Liu, L. *et al.* Anti-spike IgG causes severe acute lung injury by skewing macrophage responses during acute SARS-CoV infection. *JCI Insight* **4**, doi:10.1172/jci.insight.123158 (2019).
20 Tang, F. *et al.* Lack of peripheral memory B cell responses in recovered patients with severe acute respiratory syndrome: a six-year follow-up study. *J Immunol* **186**, 7264-7268, doi:10.4049/jimmunol.0903490 (2011).
21 Su, L. F., Kidd, B. A., Han, A., Kotzin, J. J. & Davis, M. M. Virus-specific CD4(+) memory-phenotype T cells are abundant in unexposed adults. *Immunity* **38**, 373-383, doi:10.1016/j.immuni.2012.10.021 (2013).
22 Bui, H. H. *et al.* Predicting population coverage of T-cell epitope-based diagnostics and vaccines. *BMC Bioinformatics* **7**, 153, doi:10.1186/1471-2105-7-153 (2006).
23 Vita, R. *et al.* The immune epitope database (IEDB) 3.0. *Nucleic Acids Res* **43**, D405-412, doi:10.1093/nar/gku938 (2014 Oct 9).
24 Wang, C. *et al.* The establishment of reference sequence for SARS-CoV-2 and variation analysis. *Journal of Medical Virology*, doi:10.1002/jmv.25762 (2020).
25 Phan, T. Genetic diversity and evolution of SARS-CoV-2. *Infect Genet Evol* **81**, 104260, doi:10.1016/j.meegid.2020.104260 (2020).
26 Long, Q. X. *et al.* Antibody responses to SARS-CoV-2 in patients with COVID-19. *Nat Med*, doi:10.1038/s41591-020-0897-1 (2020).
27 Vali, B. *et al.* Characterization of cross-reactive CD8+ T-cell recognition of HLA-A2-restricted HIV-Gag (SLYNTVATL) and HCV-NS5b (ALYDVVSKL) epitopes in individuals infected with human immunodeficiency and hepatitis C viruses. *J Virol* **85**, 254-263, doi:10.1128/JVI.01743-10 (2011).
28 Acierno, P. M. *et al.* Cross-reactivity between HLA-A2-restricted FLU-M1:58-66 and HIV p17 GAG:77-85 epitopes in HIV-infected and uninfected individuals. *J Transl Med* **1**, 3, doi:10.1186/1479-5876-1-3 (2003).
29 Friberg, H. *et al.* Memory CD8+ T cells from naturally acquired primary dengue virus infection are highly cross-reactive. *Immunol Cell Biol* **89**, 122-129, doi:10.1038/icb.2010.61 (2011).
30 Yin, Y. & Mariuzza, R. A. The multiple mechanisms of T cell receptor cross-reactivity. *Immunity* **31**, 849-851, doi:10.1016/j.immuni.2009.12.002 (2009).
31 Borbulevych, O. Y. *et al.* T cell receptor cross-reactivity directed by antigen-dependent tuning of peptide-MHC molecular flexibility. *Immunity* **31**, 885-896, doi:10.1016/j.immuni.2009.11.003 (2009).
32 RKI. *COVID-19 Situation Report 29/04/2020*, <https://www.rki.de/DE/Content/InfAZ/N/Neuartiges_Coronavirus/Situationsberichte/2020-04-29-en.pdf?__blob=publicationFile> (2020).
33 Dong, E., Du, H. & Gardner, L. An interactive web-based dashboard to track COVID-19 in real time. *Lancet Infect Dis* **20**, 533-534, doi:10.1016/S1473-3099(20)30120-1 (2020).
34 Kruttgen, A. *et al.* Comparison of four new commercial serologic assays for determination of SARS-CoV-2 IgG. *J Clin Virol* **128**, 104394, doi:10.1016/j.jcv.2020.104394 (2020).
35 Wilkinson, T. M. *et al.* Preexisting influenza-specific CD4+ T cells correlate with disease protection against influenza challenge in humans. *Nat Med* **18**, 274-280, doi:10.1038/nm.2612 (2012).
36 Soghoian, D. Z. *et al.* HIV-specific cytolytic CD4 T cell responses during acute HIV infection predict disease outcome. *Sci Transl Med* **4**, 123ra125, doi:10.1126/scitranslmed.3003165 (2012).
37 Messaoudi, I., Guevara Patino, J. A., Dyall, R., LeMaoult, J. & Nikolich-Zugich, J. Direct link between mhc polymorphism, T cell avidity, and diversity in immune defense. *Science* **298**, 1797-1800, doi:10.1126/science.1076064 (2002).
38 Tan, A. C., La Gruta, N. L., Zeng, W. & Jackson, D. C. Precursor frequency and competition dictate the HLA-A2-restricted CD8+ T cell responses to influenza A infection and vaccination in HLA-A2.1 transgenic mice. *J Immunol* **187**, 1895-1902, doi:10.4049/jimmunol.1100664 (2011).
39 Kiepiela, P. *et al.* CD8+ T-cell responses to different HIV proteins have discordant associations with viral load. *Nat Med* **13**, 46-53, doi:10.1038/nm1520 (2007).
40 Wu, F. *et al.* A new coronavirus associated with human respiratory disease in China. *Nature* **579**, 265-269, doi:10.1038/s41586-020-2008-3 (2020).
41 Hoof, I. *et al.* NetMHCpan, a method for MHC class I binding prediction beyond humans. *Immunogenetics* **61**, 1-13, doi:10.1007/s00251-008-0341-z (2009).
42 Nielsen, M. & Andreatta, M. NetMHCpan-3.0; improved prediction of binding to MHC class I molecules integrating information from multiple receptor and peptide length datasets. *Genome Med* **8**, 33, doi:10.1186/s13073-016-0288-x (2016).
43 Jurtz, V. *et al.* NetMHCpan-4.0: Improved Peptide-MHC Class I Interaction Predictions Integrating Eluted Ligand and Peptide Binding Affinity Data. *J Immunol* **199**, 3360-3368, doi:10.4049/jimmunol.1700893 (2017).
44 Rammensee, H., Bachmann, J., Emmerich, N. P., Bachor, O. A. & Stevanovic, S. SYFPEITHI: database for MHC ligands and peptide motifs. *Immunogenetics* **50**, 213-219, doi:10.1007/s002510050595 (1999).
45 Altschul, S. F., Gish, W., Miller, W., Myers, E. W. & Lipman, D. J. Basic local alignment search tool. *J Mol Biol* **215**, 403-410, doi:10.1016/S0022-2836(05)80360-2 (1990).
46 Johnson, M. *et al.* NCBI BLAST: a better web interface. *Nucleic Acids Res* **36**, W5-9, doi:10.1093/nar/gkn201 (2008).

47 Schlott, F. *et al.* Characterization and clinical enrichment of HLA-C*07:02-restricted Cytomegalovirus-specific CD8+ T cells. *PLoS One* **13**, e0193554, doi:10.1371/journal.pone.0193554 (2018).
48 Schmidt, A. H. *et al.* Estimation of high-resolution HLA-A, -B, -C, -DRB1 allele and haplotype frequencies based on 8862 German stem cell donors and implications for strategic donor registry planning. *Hum Immunol* **70**, 895-902, doi:10.1016/j.humimm.2009.08.006 (2009).

Figure 1

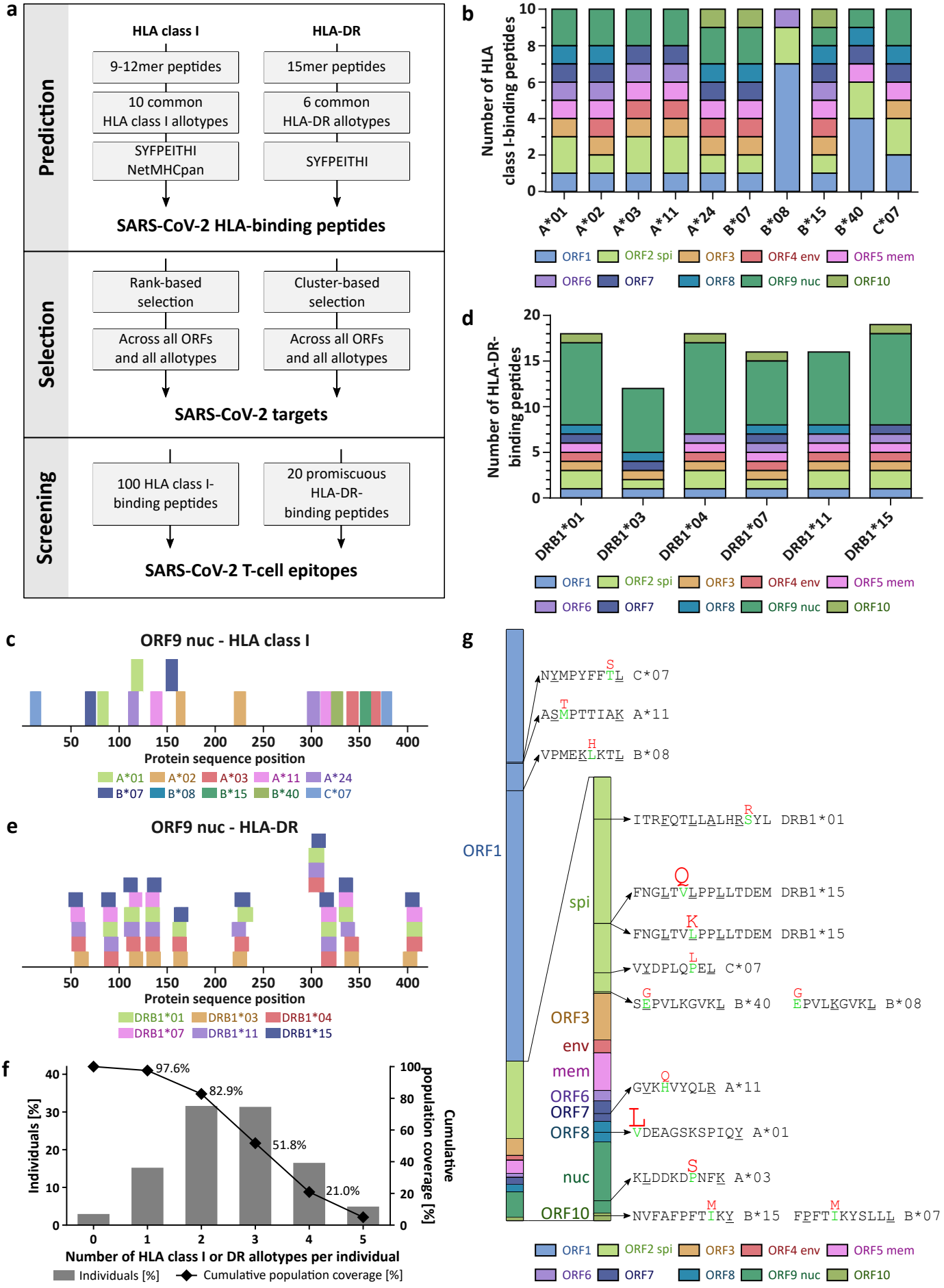
a
Prediction
HLA class I
HLA-DR
9-12mer peptides
15mer peptides
10 common HLA class I allotypes
6 common HLA-DR allotypes
SYFPEITHI NetMHCpan
SYFPEITHI
SARS-CoV-2 HLA-binding peptides
Selection
Rank-based selection
Cluster-based selection
Across all ORFs and all allotypes
Across all ORFs and all allotypes
SARS-CoV-2 targets
Screening
100 HLA class I-binding peptides
20 promiscuous HLA-DR-binding peptides
SARS-CoV-2 T-cell epitopes
b
Number of HLA class I-binding peptides
A*01 A*02 A*03 A*11 A*24 B*07 B*08 B*15 B*40 C*07
ORF1 ORF2 spi ORF3 ORF4 env ORF5 mem ORF6 ORF7 ORF8 ORF9 nuc ORF10
d
Number of HLA-DR-binding peptides
DRB1*01 DRB1*03 DRB1*04 DRB1*07 DRB1*11 DRB1*15
ORF1 ORF2 spi ORF3 ORF4 env ORF5 mem ORF6 ORF7 ORF8 ORF9 nuc ORF10
c
ORF9 nuc - HLA class I
Protein sequence position
A*01 A*02 A*03 A*11 A*24 B*07 B*08 B*15 B*40 C*07
e
ORF9 nuc - HLA-DR
Protein sequence position
DRB1*01 DRB1*03 DRB1*04 DRB1*07 DRB1*11 DRB1*15
f
Individuals [%]
Cumulative population coverage [%]
97.6%
82.9%
51.8%
21.0%
Number of HLA class I or DR allotypes per individual
Individuals [%]
Cumulative population coverage [%]
g
ORF1
spi
ORF3
env
mem
ORF6
ORF7
ORF8
nuc
ORF10
NYMPYFFTL C*07
ASMPTTIAK A*11
VPMEKLKTL B*08
ITRFQTLLALHRSYL DRB1*01
FNGLTVLPPLLTDEM DRB1*15
FNGLTVLPPLLTDEM DRB1*15
VYDPLQPEL C*07
SEPVLKGVKL B*40
EPVLKGVKL B*08
GVKHVYQLR A*11
VDEAGSKSPIQY A*01
KLDDKDPNFK A*03
NVFAFPFTIKY B*15
FPFTIKYSLLL B*07
ORF1 ORF2 spi ORF3 ORF4 env ORF5 mem ORF6 ORF7 ORF8 ORF9 nuc ORF10

Figure 1: Identification and selection of SARS-CoV-2-derived HLA class I- and HLA-DR-binding peptides. (a) Schematic overview of our prediction and selection approach to identify and finally select 120 broadly applicable SARS-CoV-2 HLA class I- and HLA-DR-binding peptides for further screening and validation as T-cell epitopes. (b, d) Selected (b) HLA class I- and (d) HLA-DR-binding peptides for the 10 and 6 most common HLA class I and HLA-DR allotypes, respectively. Each color represents a distinct ORF. spi, spike protein; env, envelope protein; mem, membrane protein; nuc, nucleocapsid protein. (c) HLA class I peptide and (e) HLA-DR peptide cluster distribution within the ORF9 nucleocapsid protein (for ORF1 - ORF8 and ORF10 refer to Extended Data Fig. 1e-m and Extended Data Fig. 2c-k). Each color represents a distinct HLA class I and HLA-DR allotype, respectively. (f) HLA allotype population coverage achieved with the selection of HLA class I and HLA-DR allotypes for SARS-CoV-2 T-cell epitope screening compared to the world population. The frequencies of individuals within the world population carrying up to five HLA class I or HLA-DR allotypes (x-axis) are indicated as grey bars on the left y-axis. The cumulative percentage of population coverage is depicted as black dots on the right y-axis. (g) Recurrent mutations[24,25] of SARS-CoV-2 ORFs within the selected peptide sequences. Wild-type and mutated amino acids are marked in green and red, respectively. Reported mutation frequencies (1 - 5%) are reflected by the size of the mutated amino acid. Anchor amino acids for HLA-binding are highlighted by underlining.

Figure 2

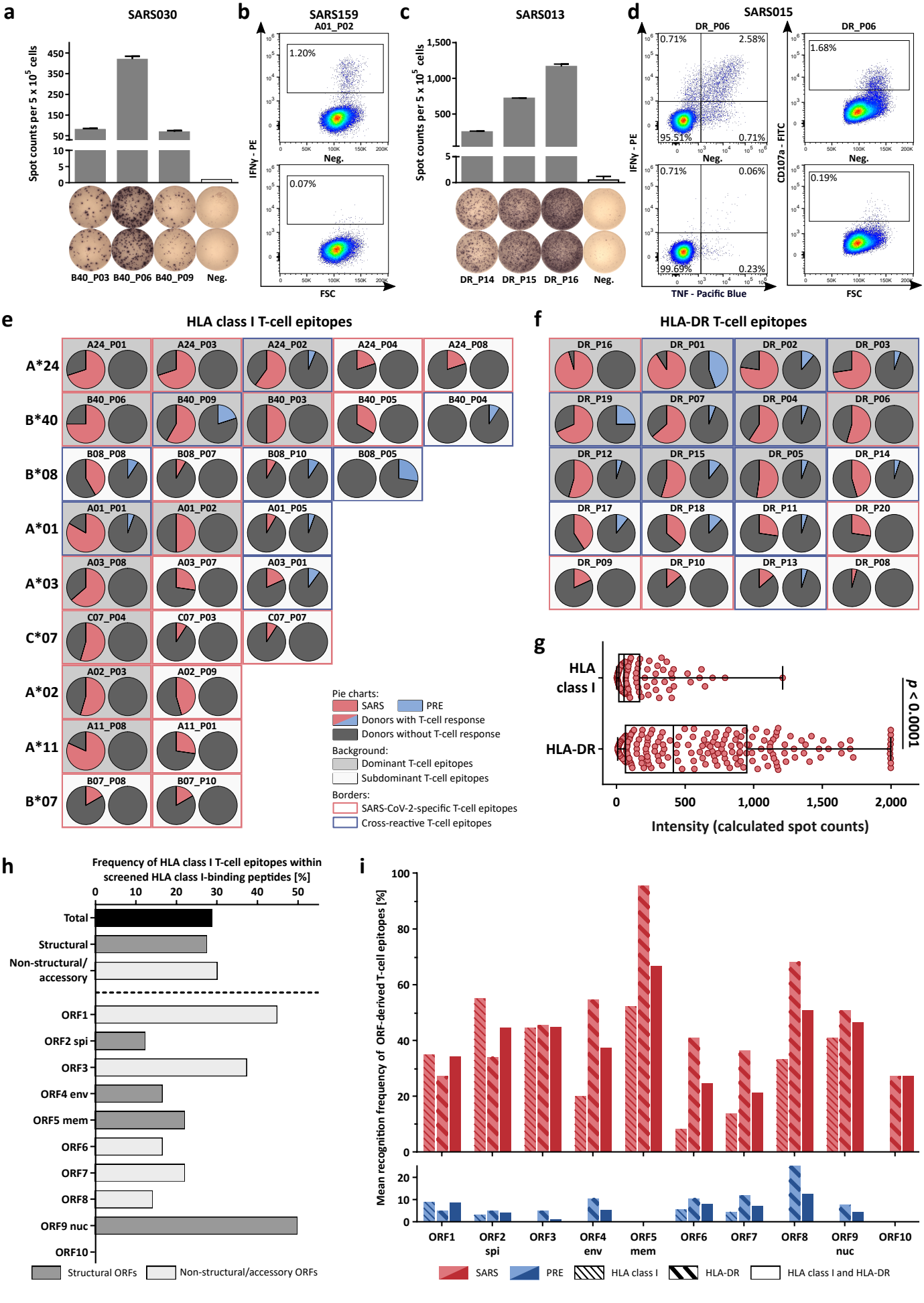
a
SARS030
Spot counts per 5 x 10^5 cells
B40_P03 B40_P06 B40_P09 Neg.
b
SARS159
A01_P02
1.20%
Neg.
0.07%
IFNγ - PE
FSC
c
SARS013
Spot counts per 5 x 10^5 cells
DR_P14 DR_P15 DR_P16 Neg.
d
SARS015
DR_P06
0.71%
2.58%
95.51%
0.71%
1.68%
0.71%
0.06%
99.69%
0.23%
0.19%
IFNγ - PE
CD107a - FITC
TNF - Pacific Blue
e
HLA class I T-cell epitopes
A*24
B*40
B*08
A*01
A*03
C*07
A*02
A*11
B*07
Pie charts:
SARS
PRE
Donors with T-cell response
Donors without T-cell response
Background:
Dominant T-cell epitopes
Subdominant T-cell epitopes
Borders:
SARS-CoV-2-specific T-cell epitopes
Cross-reactive T-cell epitopes
f
HLA-DR T-cell epitopes
g
HLA class I
HLA-DR
p < 0.0001
Intensity (calculated spot counts)
h
Frequency of HLA class I T-cell epitopes within screened HLA class I-binding peptides [%]
Total
Structural
Non-structural/ accessory
ORF1
ORF2 spi
ORF3
ORF4 env
ORF5 mem
ORF6
ORF7
ORF8
ORF9 nuc
ORF10
Structural ORFs
Non-structural/accessory ORFs
i
Mean recognition frequency of ORF-derived T-cell epitopes [%]
SARS
PRE
HLA class I
HLA-DR
HLA class I and HLA-DR

Figure 2: Validation and characterization of SARS-CoV-2-derived HLA class I and HLA-DR T-cell epitopes. (a-d) IFNγ ELISPOT assay and flow cytometry-based characterization of peptide-specific T cells from donors recovered from SARS-CoV-2 infection after *in vitro* stimulation with SARS-CoV-2-derived (a, b) HLA class I- and (c, d) HLA-DR-binding peptides. Flow cytometry data of indicated cytokines and surface markers are shown for (b) $CD8^+$ and (d) $CD4^+$ T cells. (e, f) Recognition frequency- and allotype-sorted pie charts of SARS-CoV-2-derived (e) HLA class I and (f) HLA-DR T-cell epitopes. Recognition frequency of T-cell epitopes in groups of HLA class I-matched convalescent donors of SARS-CoV-2 infection (SARS group 1, total n = 116, left pie chart, red) and donors never exposed to SARS-CoV-2 (PRE group A, total n = 104, right pie chart, blue) were assessed by ELISPOT assays. Dominant (immune responses in ≥ 50% of SARS donors) and subdominant T-cell epitopes are marked with dark grey and light grey background, respectively. SARS-CoV-2-specific T-cell epitopes with responses detected exclusively in the SARS group are marked with a red frame, cross-reactive epitopes with immune responses detected in the PRE group are marked with a blue frame. (g) Calculated spot counts were assessed by ELISPOT assays of SARS-CoV-2-derived HLA class I (n = 121) and HLA-DR T-cell epitopes (n = 214) in the SARS group (min/max box plots, Mann-Whitney U test). (h) Frequency of validated HLA class I T-cell epitopes for structural (dark grey) and non-structural/accessory (light grey) ORFs. spi, spike protein; env, envelope protein; mem, membrane protein; nuc, nucleocapsid protein. (i) Mean recognition frequency of HLA class I and HLA-DR T-cell epitopes by SARS (red) and PRE donors (blue) within the different ORFs.

Figure 3

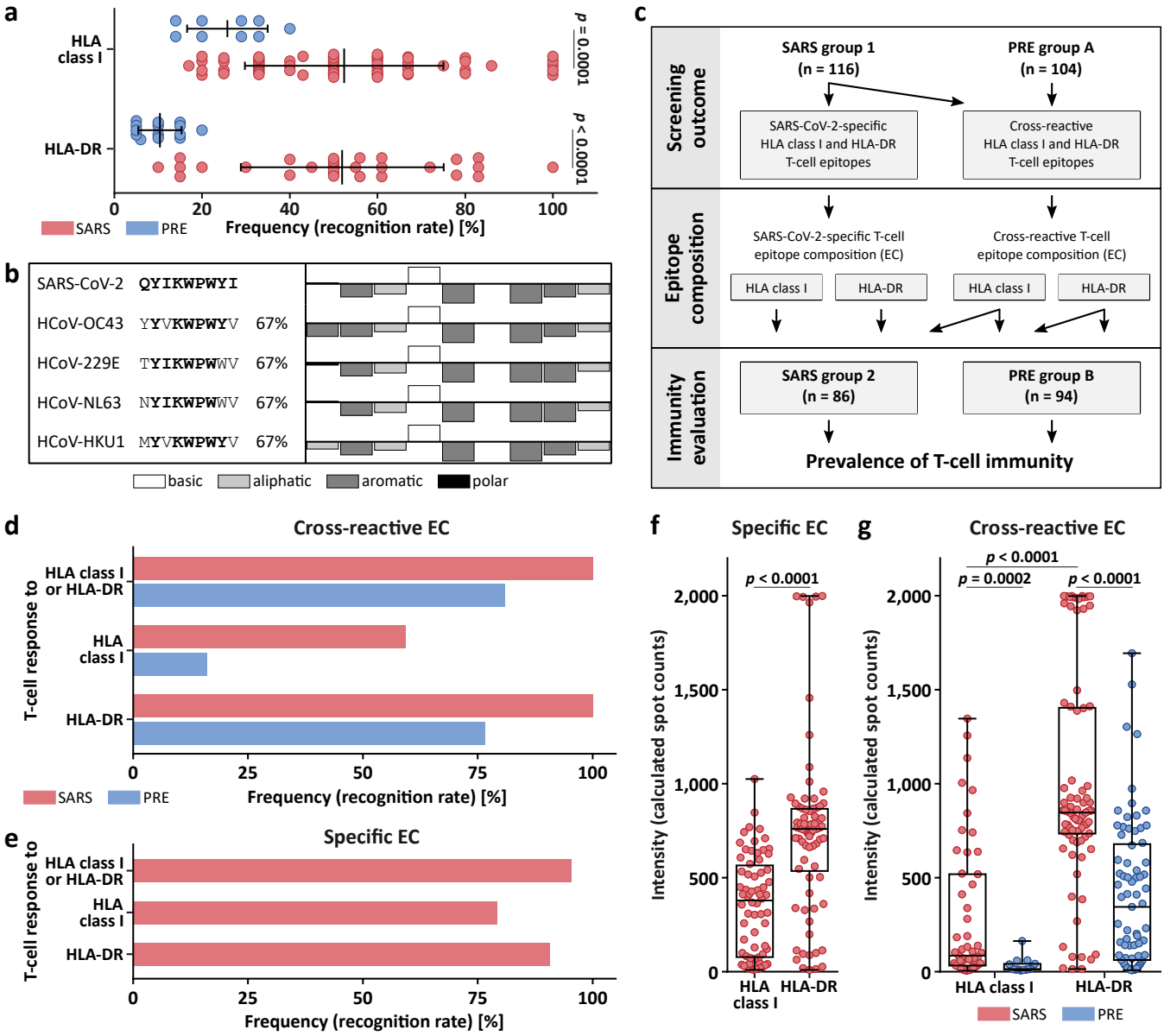
a
HLA class I
HLA-DR
p = 0.0001
p < 0.0001
0
20
40
60
80
100
SARS
PRE
Frequency (recognition rate) [%]
b
SARS-CoV-2 QYIKWPWYI
HCoV-OC43 YYVKWPWYV 67%
HCoV-229E TYIKWPWWV 67%
HCoV-NL63 NYIKWPWWV 67%
HCoV-HKU1 MYVKWPWYV 67%
basic
aliphatic
aromatic
polar
c
Screening outcome
SARS group 1 (n = 116)
PRE group A (n = 104)
SARS-CoV-2-specific HLA class I and HLA-DR T-cell epitopes
Cross-reactive HLA class I and HLA-DR T-cell epitopes
Epitope composition
SARS-CoV-2-specific T-cell epitope composition (EC)
Cross-reactive T-cell epitope composition (EC)
HLA class I
HLA-DR
HLA class I
HLA-DR
Immunity evaluation
SARS group 2 (n = 86)
PRE group B (n = 94)
Prevalence of T-cell immunity
d
Cross-reactive EC
T-cell response to
HLA class I or HLA-DR
HLA class I
HLA-DR
0
25
50
75
100
SARS
PRE
Frequency (recognition rate) [%]
e
Specific EC
T-cell response to
HLA class I or HLA-DR
HLA class I
HLA-DR
0
25
50
75
100
Frequency (recognition rate) [%]
f
Specific EC
p < 0.0001
Intensity (calculated spot counts)
2,000
1,500
1,000
500
0
HLA class I
HLA-DR
g
Cross-reactive EC
p < 0.0001
p = 0.0002
p < 0.0001
Intensity (calculated spot counts)
2,000
1,500
1,000
500
0
HLA class I
HLA-DR
SARS
PRE

Figure 3: Detection and characterization of T-cell responses to SARS-CoV-2-derived HLA class I and HLA-DR T-cell epitopes in unexposed individuals. (a) Recognition rate of HLA class I and HLA-DR SARS-CoV-2 T-cell epitopes in SARS group 1 (n = 116) and PRE group A (n = 104), respectively (data shown for donors with T-cell responses, Mann-Whitney U test). (b) Representative sequence and physiochemical property alignments of the cross-reactive SARS-CoV-2 T-cell epitope A24_P02 with the four seasonal common cold human coronaviruses (HCoV-OC43, HCoV-229E, HCoV-NL63, HCoV-HKU1, for other cross-reactive peptides refer to Supplementary Tables 9 and 10, Supplementary Data 1). Physiochemical properties were calculated by the PepCalc software. Column directions (up vs. down) indicate hydrophilicity according to the Hopp-Woods scale. (c) Schematic overview of the definition of SARS-CoV-2-specific and cross-reactive epitope compositions (EC) for standardized evaluation of SARS-CoV-2 T-cell responses in a group of convalescents from SARS-CoV-2 infection (SARS group 2, n = 86) and a group of unexposed individuals (PRE group B, n = 94). (d, e) Recognition frequency of (d) cross-reactive and (e) SARS-CoV-2-specific EC by T cells in the SARS group 2 and PRE group B. (f, g) Calculated spot counts for (f) SARS-CoV-2-specific (HLA class I: n = 68; HLA-DR: n = 78) and (g) cross-reactive EC in the SARS group 2 (HLA class I: n = 51; HLA-DR: n = 86) and PRE group B (HLA class I: n = 15; HLA-DR: n = 73) (min/max box plots, Mann-Whitney U test).

Figure 4

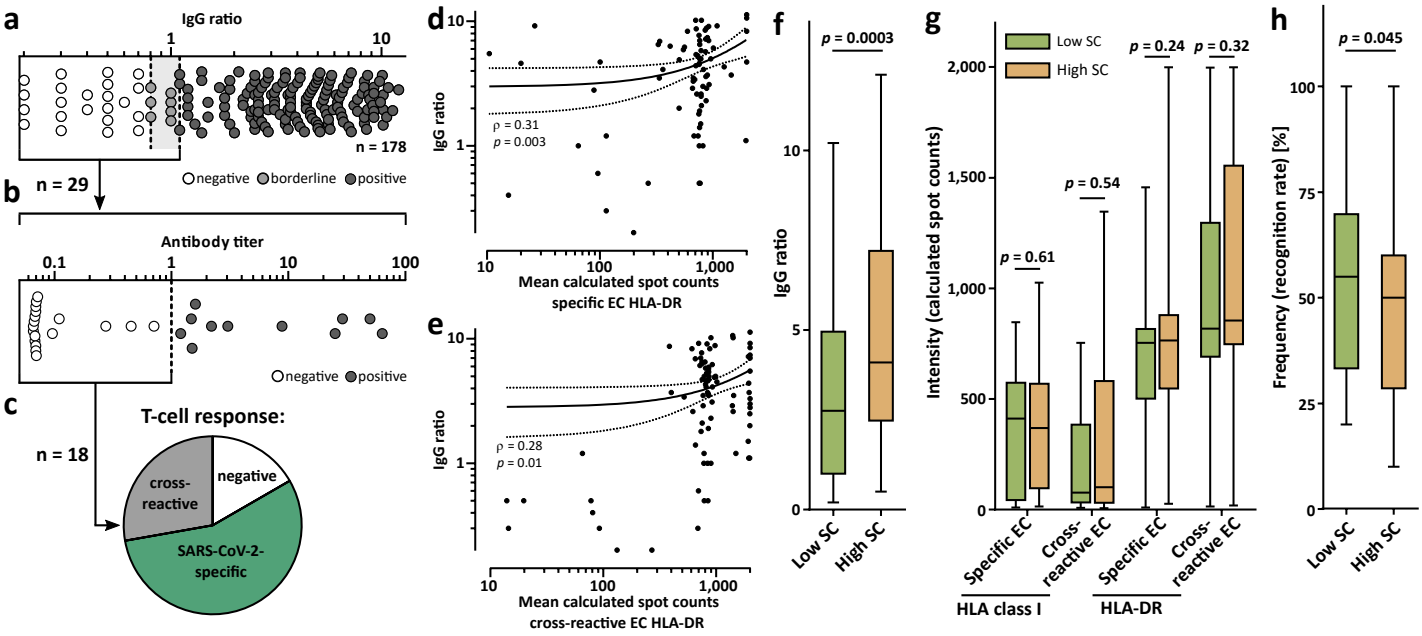
a
IgG ratio
1
10
n = 178
negative borderline positive
b
n = 29
Antibody titer
0.1
1
10
100
negative positive
c
n = 18
T-cell response:
cross-reactive
negative
SARS-CoV-2-specific
d
IgG ratio
ρ = 0.31
p = 0.003
Mean calculated spot counts specific EC HLA-DR
e
IgG ratio
ρ = 0.28
p = 0.01
Mean calculated spot counts cross-reactive EC HLA-DR
f
p = 0.0003
IgG ratio
Low SC
High SC
g
Low SC
High SC
Intensity (calculated spot counts)
p = 0.61
p = 0.54
p = 0.24
p = 0.32
Specific EC
Cross-reactive EC
Specific EC
Cross-reactive EC
HLA class I
HLA-DR
h
p = 0.045
Frequency (recognition rate) [%]
Low SC
High SC

Figure 4: SARS-CoV-2-directed antibody and T-cell responses in the course of COVID-19. (a, b) SARS-CoV-2 serum (a) IgG S1 ratio (EUROIMMUN) in SARS donors (n = 178) and (b) anti-nucleocapsid antibody titers (Elecsys® immunoassay) of SARS donors with borderline/negative responses in EUROIMMUN assay (n = 29). Donors with negative/borderline responses are marked in white or grey, respectively. (c) The pie chart displays T-cell responses (positive: n = 15; negative: n = 3) to SARS-CoV-2-specific (n = 10) and cross-reactive (n = 5) T-cell epitopes in donors without antibody responses (n = 18, assessed in two independent assays). (d, e) Correlation analysis of IgG ratios (EUROIMMUN) to SARS-CoV-2 with spot counts assessed by ELISPOT assays for HLA-DR (d) SARS-CoV-2-specific (n = 78) and (e) cross-reactive (n = 86) epitope composition (EC) in SARS group 2 (dotted lines: 95% confidence level, Spearman's rho (ρ) and *p*-value). (f) IgG antibody response (EUROIMMUN) to SARS-CoV-2 (n = 178) and (g) T-cell response to SARS-CoV-2-specific (HLA class I: n = 68; HLA-DR: n = 78) and cross-reactive EC (HLA class I: n = 51; HLA-DR: n = 86), respectively, in SARS donors with low and high symptom score (SC, combining objective (fever ≥ 38°C) and subjective disease symptoms) in the course of COVID-19. (h) Recognition rate of T-cell epitopes in SARS donors (group 1) with low and high SC in the course of COVID-19 (n = 84). (f, g) min/max box plots, Mann-Whitney U test, (h) min/max box plots, one-sided t test.

Extended Data Figure 1

a

ORF	ORF length [aa]	# 9-12mers	# HLA class I peptides
ORF1	7,096	28,346	1,327
ORF2 spi	1,273	5,054	192
ORF3	275	1,062	52
ORF4 env	75	262	17
ORF5 mem	222	850	43
ORF6	61	206	16
ORF7	121	446	20
ORF8	121	446	13
ORF9 nuc	419	1,638	52
ORF10	38	114	7
total	**9,701**	**38,424**	**1,739**

b

ORF	A*01	A*02	A*03	A*11	A*24	B*07	B*08	B*15	B*40	C*07
ORF1	106	285	248	240	183	102	26	173	30	143
ORF2 spi	13	32	32	44	24	17	3	31	4	19
ORF3	3	17	7	9	9	6	0	5	0	4
ORF4 env	0	7	2	2	2	1	0	4	0	0
ORF5 mem	3	6	6	10	9	2	0	4	1	10
ORF6	1	7	5	2	0	0	1	2	0	0
ORF7	1	6	2	2	3	2	0	3	1	2
ORF8	1	4	0	0	2	1	0	2	1	3
ORF9 nuc	5	5	14	10	4	9	0	7	1	2
ORF10	0	0	0	0	4	2	0	1	0	0
total	**133**	**369**	**316**	**319**	**240**	**142**	**30**	**232**	**38**	**183**

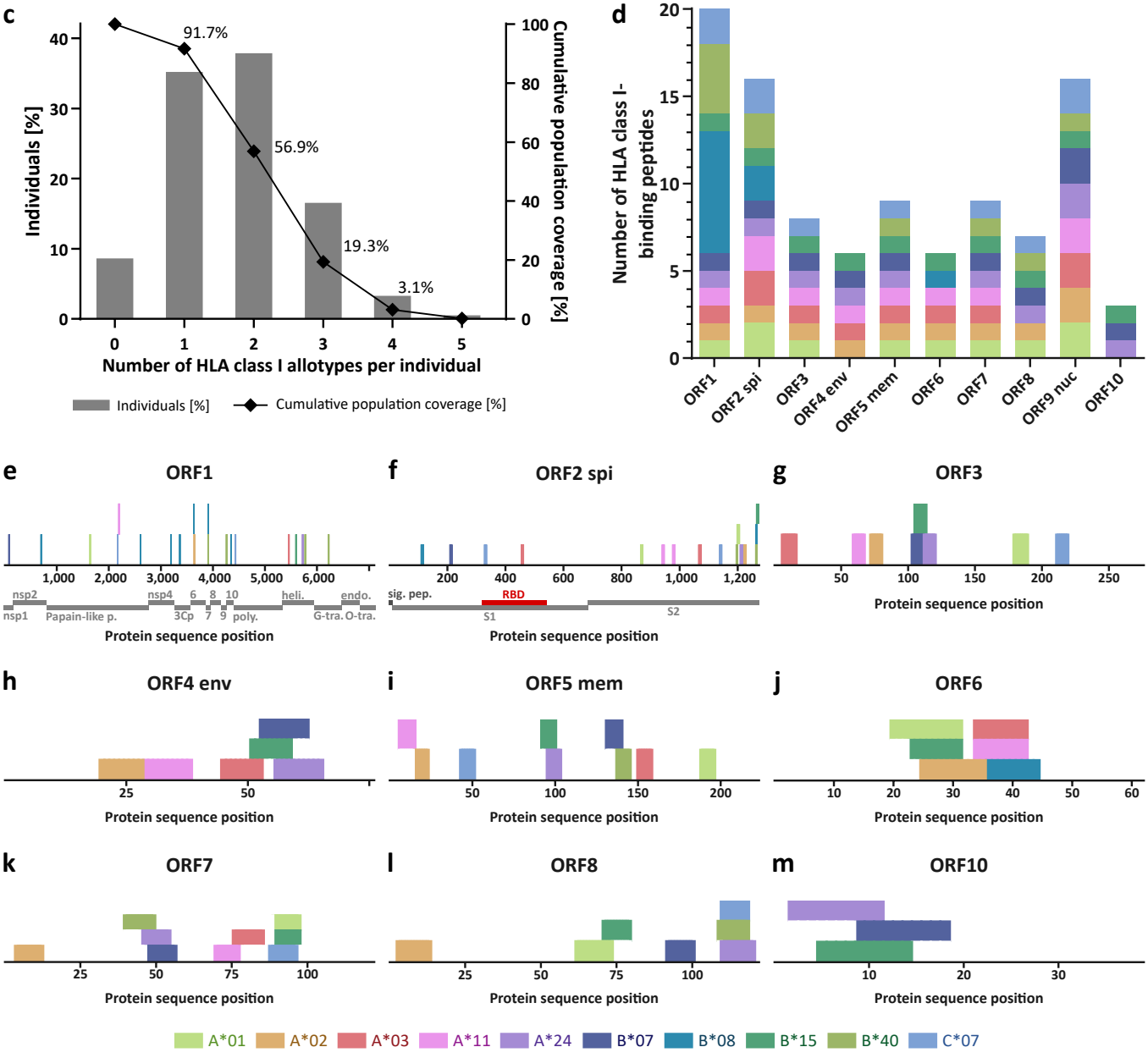

Extended Data Figure 1: Prediction of SARS-CoV-2-derived HLA class I-binding peptides. (a) Overview of amino acid lengths of SARS-CoV-2 ORFs, total number of 9 - 12 amino acid long peptides, and number of predicted HLA class I-binding peptides. aa, amino acid; spi, spike protein; env, envelope protein; mem, membrane protein; nuc, nucleocapsid protein. (b) Number of predicted HLA class I-binding peptides for each HLA class I allotype. (c) HLA class I allotype population coverage achieved with the selection of HLA class I allotypes compared to the world population. The frequencies of individuals within the world population carrying up to five HLA allotypes (x-axis) are indicated as grey bars on the left y-axis. The cumulative percentage of population coverage is depicted as black dots on the right y-axis. (d) Distribution of different HLA class I-restricted peptides within SARS-CoV-2 ORFs. Each color represents a distinct HLA class I allotype. (e-m) HLA class I-binding peptide distribution within the different SARS-CoV-2 ORFs. Chains (grey) and domains (red) of ORF1 and ORF2 are indicated. Each color represents a distinct HLA class I allotype. nsp, non-structural protein; p, proteinase; poly.; polymerase; heli., helicase; G-tra., Guanine-N7 methyltransferase; endo., endoribonuclease; O-tra., 2'-O-methyltransferase; sig. pep., signal peptide; RBD, receptor binding domain.

Extended Data Figure 2

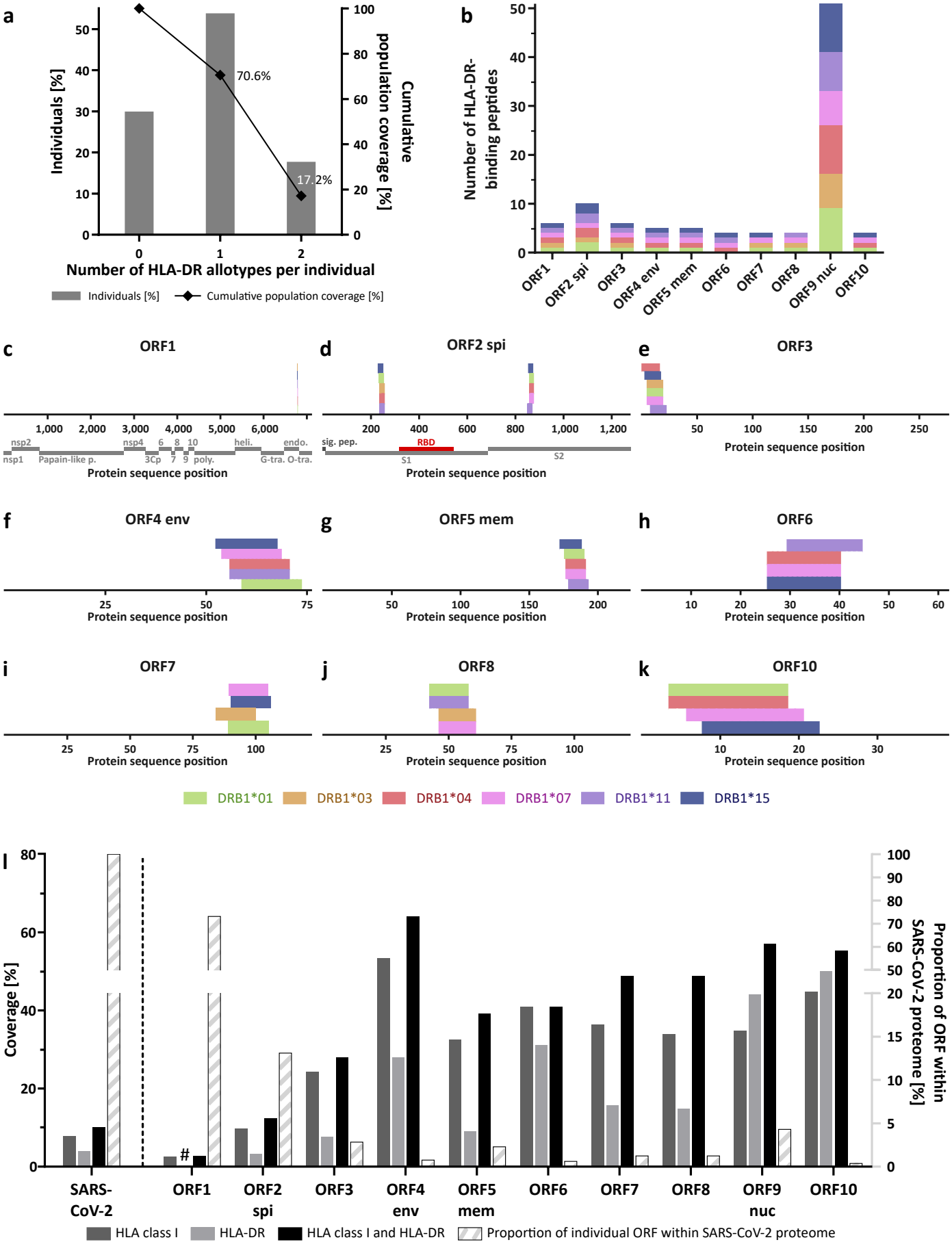

Extended Data Figure 2: Prediction of SARS-CoV-2-derived HLA-DR-binding peptides and ORF coverage with predicted HLA class I- and HLA-DR-binding peptides. (a) HLA-DR allotype population coverage achieved with the selection of HLA-DR allotypes compared to the world population. The frequencies of individuals within the world population carrying up to two HLA-DR allotypes (x-axis) are indicated as grey bars on the left y-axis. The cumulative percentage of population coverage is depicted as black dots on the right y-axis. (b) Number of predicted HLA-DR-binding peptides for each HLA-DR allotype covered with the selected peptide clusters. Each color represents a distinct HLA-DR allotype. spi, spike protein; env, envelope protein; mem, membrane protein; nuc, nucleocapsid protein. (c-k) Distribution of peptide clusters selected for immunogenicity screening within the different SARS-CoV-2 ORFs. Chains (grey) and domains (red) of ORF1 and ORF2 are indicated. Each color represents a distinct HLA-DR allotype. nsp, non-structural protein; p, proteinase; poly., polymerase; heli., helicase; G-tra., Guanine-N7 methyltransferase; endo., endoribonuclease; O-tra., 2'-O-methyltransferase; sig. pep., signal peptide; RBD, receptor binding domain. (l) Protein coverage of total SARS-CoV-2 proteome and individual SARS-CoV-2 ORFs with selected HLA class I- and HLA-DR-binding peptides (left y-axis). Striped bars indicate the proportion of individual ORF protein lengths within the total SARS-CoV-2 proteome (right y-axis). The protein coverage of HLA-DR-derived peptides for ORF1 (marked with #) amounts to 0.3%.

Extended Data Figure 3

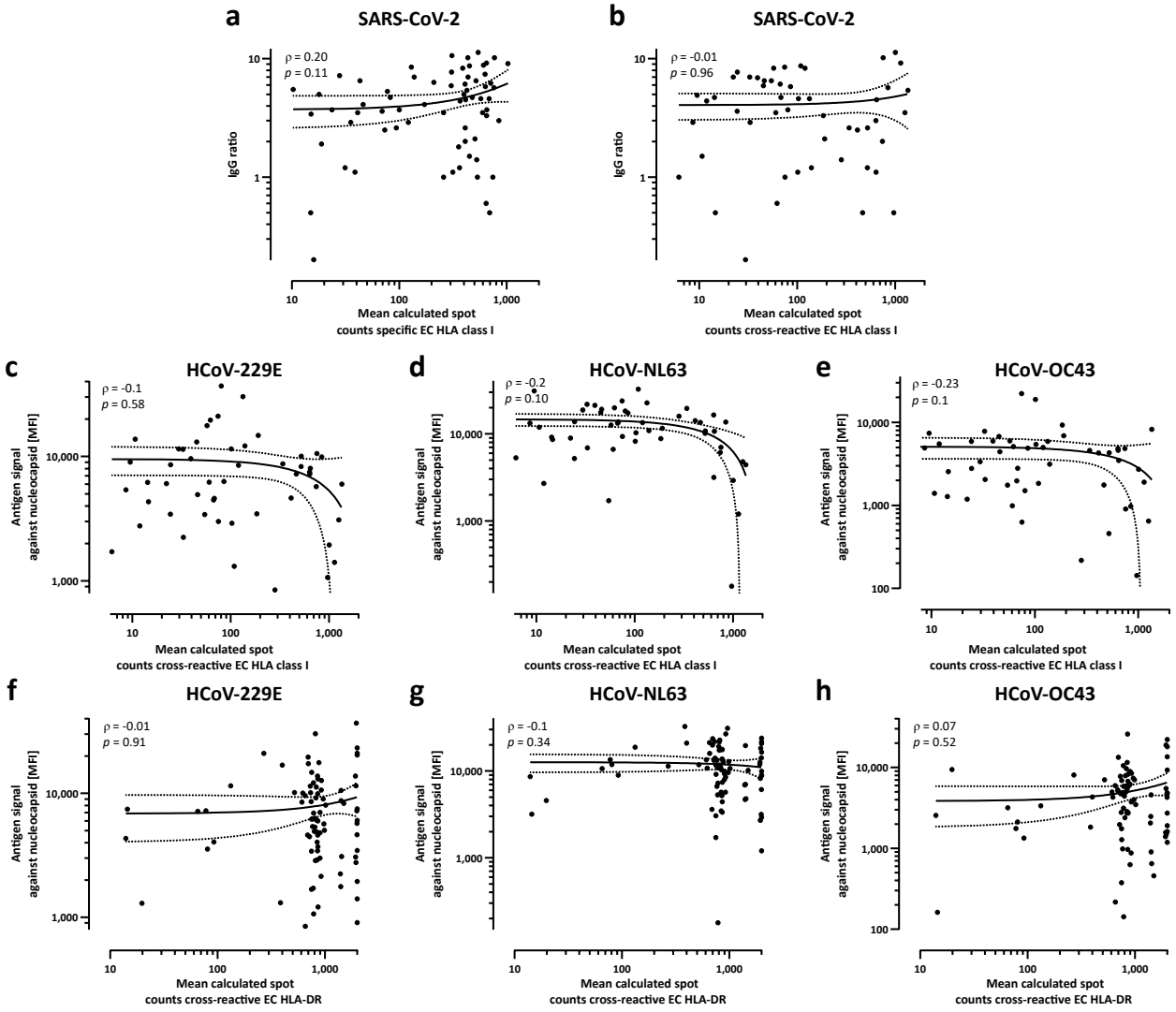

Extended Data Figure 3: Correlation of antibody response with measured T-cell intensity. (a, b) Correlation analysis of IgG serum ELISA ratios (EUROIMMUN) to SARS-CoV-2 and calculated spot counts assessed in IFNγ ELISPOT assays for HLA class I-restricted (a) SARS-CoV-2-specific (n = 68) and (b) cross-reactive (n = 51) epitope compositions (EC) in SARS group 2 (dotted lines: 95% confidence level, Spearmans rho (ρ) and *p*-value). (c-h) Correlation analysis of IgG (MFI signals) to nucleocapsid protein of three common cold coronaviruses (HCoV-OC43, HCoV-229E, HCoV-NL63) and calculated spot counts assessed in IFNγ ELISPOT assays for (c-e) HLA class I (n = 51) and (f-h) HLA-DR (n = 86) cross-reactive EC in SARS group 2 (dotted lines: 95% confidence level, Spearmans rho (ρ) and *p*-value).

Extended Data Figure 4

a

Logistic regression analysis for SC in SARS cohort 2

	OR (95% CI)	P value
Age		
≤ 30	1	
31 - 49	17.1 (2.5 - 116.6)	0.004
≥ 50	20.0 (3.2 - 125.4)	0.001
Gender		
Female	1	
Male	1.8 (0.4 - 8.5)	0.4
BMI (kg/m²)		
≤ 24	1	
25 - 29	0.4 (0.07 - 2.0)	0.2
≥ 30	0.9 (0.06 - 12.4)	0.9
Specific EC HLA class I	1 (0.99 - 1.003)*	0.6
Specific EC HLA-DR	1 (0.99 - 1.002)*	0.9
IgG ratio	1.3 (0.99 - 1.8)*	0.04

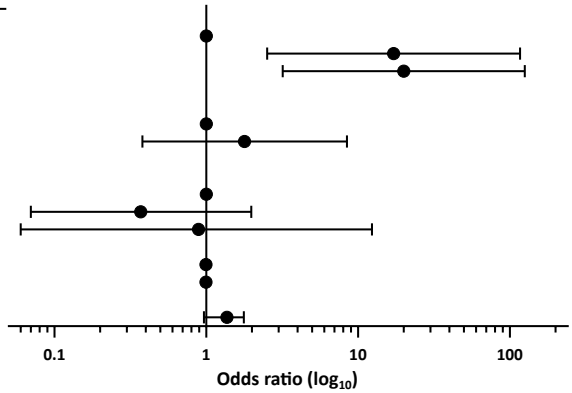

b

Logistic regression analysis for SC in SARS cohort 1

	OR (95% CI)	P value
Age		
≤ 30	1	
31 - 49	7.2 (1.2 - 42.5)	0.03
≥ 50	6.8 (1.1 - 44.6)	0.04
Gender		
Female	1	
Male	1.1 (0.3 - 4.6)	0.9
BMI (kg/m²)		
≤ 24	1	
25 - 29	2.5 (0.5 - 12.2)	0.3
≥ 30	0.5 (0.1 - 2.9)	0.4
Recognition rate [%]	0.01 (0.0003 - 0.6)*	0.02
IgG ratio	2.0 (1.4 - 3.0)*	< 0.0001

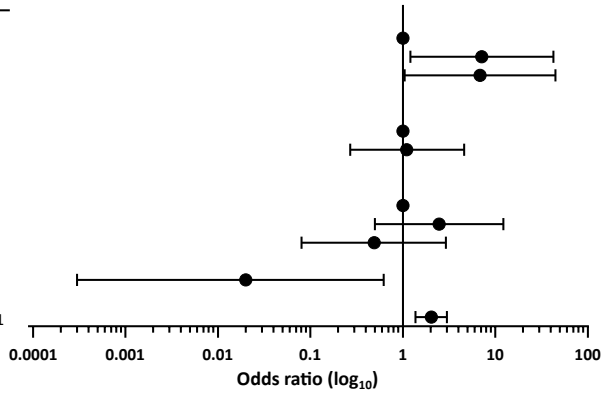

Extended Data Figure 4: Predictors of symptom severity in patient collection. (a, b) Odds ratios (ORs) for age, gender, BMI groups, IgG antibody responses (EUROIMMUN), and (a) intensity of T-cell responses to HLA class I and HLA-DR SARS-CoV-2-specific EC or (b) recognition rate based on an adjusted model of predictors for low vs. high symptom score (SC) in SARS donors of group (a) 2 and (b) 1, respectively. * adjusted OR per unit increase in continuous variable.

Extended Data Table 1: Donor characteristics

	SARS collection (n = 180)		PRE collection (n = 185)	
	group 1	**group 2**	**group A**	**group B**
Number of donors	116	86	104	94
Age [years]				
Range	18 - 75	18 - 75	21 - 70	21 - 68
Median	44	44	45	50
n.a.	-	-	5	1
Sex [n (%)]				
Female	55 (47)	44 (51)	23 (23)	21 (22)
Male	61 (53)	42 (49)	77 (77)	73 (78)
n.a.	-	-	4	-
Sample collection date	04/2020 - 05/2020	04/2020 - 05/2020	06/2007 - 11/2019	05/2017 - 05/2019
SARS-CoV-2 PCR positivity [n (%)]	116 (100)	86 (100)	n.a.	n.a.
Antibody response [n (%)]				
positive	96 (84)	71 (83)	n.a.	n.a.
negative	18 (16)	15 (17)		
n.a.	2	0		
Interval positive test to sample collection [days]			n.a.	n.a.
Range	19 - 52	30 - 59		
Mean	37.7	43.5		
Awareness of symptoms [n (%)]				
No	10 (9)	6 (7)		
Mild	26 (22)	13 (15)	n.a.	n.a.
Moderate	52 (45)	47 (55)		
Severe	28 (24)	20 (23)		
Febrile illness (≥ 38.0°C)				
Yes	62 (53)	50 (58)	n.a.	n.a.
No	54 (47)	36 (42)		
Symptom score [n (%)]				
Low SC	50 (43)	36 (42)	n.a.	n.a.
High SC	66 (57)	50 (58)		
Hospitalized patients [n (%)]	3 (3)	2 (2)	n.a.	n.a.
Past medical history [n (%)]				
Arterial hypertension	12 (10)	12 (14)		
Preexisting autoimmune disease	9 (8)	7 (8)		
Intake of immunosuppressive drugs	5 (4)	6 (7)		
Diabetes mellitus	1 (1)	1 (1)	n.a.	n.a.
Malignant disease	4 (3)	3 (4)		
Liver disease	1 (1)	0 (0)		
Lung disease	3 (3)	4 (5)		
Smoking	11 (10)	7 (8)		

Antibody response indicates EUROIMMUNE test results. Awareness of symptoms indicates patient-subjective disease severity. Symptom score was determined by combining objective (fever ≥ 38.0°C) and subjective disease symptoms. n, number; n.a., not available; SC, symptom score.

Extended Data Table 1: Donor characteristics

This table summarizes the donor characteristics of the SARS groups 1 and 2 as well as of the PRE groups A and B.

Extended Data Table 2: Immunogenic SARS-CoV-2-derived HLA class I T-cell epitopes

Peptide ID	Sequence	Protein	Protein class	HLA restriction	SARS group 1 [positive/tested (%)]	PRE group A [positive/tested (%)]
A01_P01	TTDPSFLGRY	ORF1	non-structural	A*01	**10/12 (83%)**	1/18 (6%)
A01_P02	LTDEMIAQY	ORF2 spi	structural	A*01	**6/12 (50%)**	0/18 (0%)
A01_P05	RTFKVSIWNLDY	ORF6	accessory	A*01	1/12 (8%)	1/18 (6%)
A02_P03	ALSKGVHFV	ORF3	accessory	A*02	**6/11 (55%)**	0/8 (0%)
A02_P09	LLLLDRLNQL	ORF9 nuc	structural	A*02	5/11 (45%)	0/8 (0%)
A03_P01	KLFAAETLK	ORF1	non-structural	A*03	2/11 (18%)	1/10 (10%)
A03_P07	QLRARSVSPK	ORF7	accessory	A*03	3/11 (27%)	0/10 (0%)
A03_P08	KTFPPTEPKK	ORF9 nuc	structural	A*03	**7/11 (64%)**	0/10 (0%)
A11_P01	ASMPTTIAK	ORF1	non-structural	A*11	3/11 (27%)	0/9 (0%)
A11_P08	ATEGALNTPK	ORF9 nuc	structural	A*11	**9/11 (82%)**	0/9 (0%)
A24_P01	VYIGDPAQL	ORF1	non-structural	A*24	**7/10 (70%)**	0/17 (0%)
A24_P02	QYIKWPWYI	ORF2 spi	structural	A*24	**6/10 (60%)**	1/16 (6%)
A24_P03	VYFLQSINF	ORF3	accessory	A*24	**7/10 (70%)**	0/17 (0%)
A24_P04	FYVYSRVKNL	ORF4 env	structural	A*24	2/10 (20%)	0/17 (0%)
A24_P08	DYKHWPQIAQF	ORF9 nuc	structural	A*24	2/10 (20%)	0/16 (0%)
B07_P08	FPRGQGVPI	ORF9 nuc	structural	B*07	2/12 (17%)	0/9 (0%)
B07_P10	NPANNAAIVL	ORF9 nuc	structural	B*07	2/12 (17%)	0/9 (0%)
B08_P05	TPKYKFVRI	ORF1	non-structural	B*08	0/12 (0%)	3/11 (27%)
B08_P07	FVKHKHAFL	ORF1	non-structural	B*08	1/12 (8%)	0/11 (0%)
B08_P08	DLKGKYVQI	ORF1	non-structural	B*08	5/12 (42%)	1/11 (9%)
B08_P10	EAFEKMVSL	ORF1	non-structural	B*08	1/12 (8%)	1/11 (9%)
B40_P03	SELVIGAVIL	ORF5 mem	structural	B*40	**6/12 (50%)**	0/11 (0%)
B40_P04	YEGNSPFHPL	ORF7	accessory	B*40	0/12 (0%)	1/11 (9%)
B40_P05	LEYHDVRVVL	ORF8	accessory	B*40	4/12 (33%)	0/11 (0%)
B40_P06	MEVTPSGTWL	ORF9 nuc	structural	B*40	**9/12 (75%)**	0/11 (0%)
B40_P09	IEYPIIGDEL	ORF1	non-structural	B*40	**7/12 (58%)**	2/10 (20%)
C07_P03	YYQLYSTQL	ORF3	accessory	C*07	1/11 (9%)	0/9 (0%)
C07_P04	NRFLYIIKL	ORF5 mem	structural	C*07	**6/11 (55%)**	0/9 (0%)
C07_P07	QRNAPRITF	ORF9 nuc	structural	C*07	1/11 (9%)	0/9 (0%)

Dominant T-cell epitopes (immune responses in ≥ 50% of SARS donors) are marked in bold. ID, identification number; spi, spike protein; env, envelope protein; mem, membrane protein; nuc, nucleocapsid protein.

Extended Data Table 2: Immunogenic SARS-CoV-2-derived HLA class I T-cell epitopes

This table shows immunogenic SARS-CoV-2-derived HLA class I T-cell epitopes with detected recognition frequencies in the SARS and PRE group.

Extended Data Table 3: Immunogenic SARS-CoV-2-derived HLA-DR T-cell epitopes

Peptide ID	Sequence	Protein	Protein class	SARS group 1 [positive/tested (%)]	PRE group A [positive/tested (%)]
DR_P01	KDGIIWVATEGALNT	ORF9 nuc	structural	**20/22 (91%)**	8/18 (44%)
DR_P02	GTWLTYTGAIKLDDK	ORF9 nuc	structural	**17/22 (77%)**	2/18 (11%)
DR_P03	RWYFYYLGTGPEAGL	ORF9 nuc	structural	**16/22 (73%)**	1/18 (6%)
DR_P04	ASWFTALTQHGKEDL	ORF9 nuc	structural	**13/22 (59%)**	1/18 (6%)
DR_P05	ASAFFGMSRIGMEVT	ORF9 nuc	structural	**12/23 (52%)**	1/18 (6%)
DR_P06	IGYYRRATRRIRGGD	ORF9 nuc	structural	**12/22 (55%)**	0/17 (0%)
DR_P07	LLLLDRLNQLESKMS	ORF9 nuc	structural	**14/22 (64%)**	1/17 (6%)
DR_P08	AADLDDFSKQLQQSM	ORF9 nuc	structural	1/23 (4%)	0/17 (0%)
DR_P09	AIVLQLPQGTTLPKG	ORF9 nuc	structural	4/22 (18%)	0/17 (0%)
DR_P10	YKHWPQIAQFAPSAS	ORF9 nuc	structural	3/22 (14%)	0/16 (0%)
DR_P11	LDDFVEIIKSQDLSV	ORF1	non-structural	6/22 (27%)	1/20 (5%)
DR_P12	ITRFQTLLALHRSYL	ORF2 spi	structural	**12/22 (55%)**	1/20 (5%)
DR_P13	FNGLTVLPPLLTDEM	ORF2 spi	structural	3/22 (14%)	1/20 (5%)
DR_P14	FMRIFTIGTVTLKQG	ORF3	accessory	10/22 (45%)	1/20 (5%)
DR_P15	FYVYSRVKNLNSSRV	ORF4 env	structural	**12/22 (55%)**	2/19 (11%)
DR_P16	LSYYKLGASQRVAGD	ORF5 mem	structural	**21/22 (95%)**	0/19 (0%)
DR_P17	IWNLDYIINLIIKNL	ORF6	accessory	9/22 (41%)	2/19 (11%)
DR_P18	QEEVQELYSPIFLIV	ORF7	accessory	8/22 (36%)	2/17 (12%)
DR_P19	SKWYIRVGARKSAPL	ORF8	accessory	**15/22 (68%)**	4/16 (25%)
DR_P20	INVFAFPFTIYSLLL	ORF10	accessory	6/22 (27%)	0/15 (0%)

Dominant T-cell epitopes (immune responses in ≥ 50% of SARS donors) are marked in bold. ID, identification number; spi, spike protein; env, envelope protein; mem, membrane protein; nuc, nucleocapsid protein.

Extended Data Table 3: Immunogenic SARS-CoV-2-derived HLA-DR T-cell epitopes

This table reports immunogenic SARS-CoV-2-derived HLA-DR T-cell epitopes with detected recognition frequencies in the SARS and PRE group.

Extended Data Table 4: SARS-CoV-2-specific and cross-reactive HLA class I and HLA-DR T-cell epitope compositions

HLA class I T-cell epitope compositions

SARS-CoV-2-specific EC				Cross-reactive EC			
Peptide ID	**Sequence**	**ORF**	**HLA restriction**	**Peptide ID**	**Sequence**	**ORF**	**HLA restriction**
A01_P02	LTDEMIAQY	ORF2 spi	A*01	A01_P01	TTDPSFLGRY	ORF1	A*01
A02_P03	ALSKGVHFV	ORF3	A*02	A01_P05	RTFKVSIWNLDY	ORF6	A*01
A02_P09	LLLLDRLNQL	ORF9 nuc	A*02	A03_P01	KLFAAETLK	ORF1	A*03
A03_P07	QLRARSVSPK	ORF7	A*03	A24_P02	QYIKWPWYI	ORF2 spi	A*24
A03_P08	KTFPPTEPKK	ORF9 nuc	A*03	B08_P05	TPKYKFVRI	ORF1	B*08
A11_P01	ASMPTTIAK	ORF1	A*11	B08_P08	DLKGKYVQI	ORF1	B*08
A11_P08	ATEGALNTPK	ORF9 nuc	A*11	B08_P10	EAFEKMVSL	ORF1	B*08
A24_P01	VYIGDPAQL	ORF1	A*24	B40_P04	YEGNSPFHPL	ORF7	B*40
A24_P03	VYFLQSINF	ORF3	A*24	B40_P09	IEYPIIGDEL	ORF1	B*40
B07_P08	FPRGQGVPI	ORF9 nuc	B*07				
B07_P10	NPANNAAIVL	ORF9 nuc	B*07				
B08_P07	FVKHKHAFL	ORF1	B*08				
B40_P03	SELVIGAVIL	ORF5 mem	B*40				
B40_P06	MEVTPSGTWL	ORF9 nuc	B*40				
C07_P03	YYQLYSTQL	ORF3	C*07				
C07_P04	NRFLYIIKL	ORF5 mem	C*07				

HLA-DR T-cell epitope compositions

SARS-CoV-2-specific EC				Cross-reactive EC			
Peptide ID	**Sequence**	**ORF**	**HLA restriction**	**Peptide ID**	**Sequence**	**ORF**	**HLA restriction**
DR_P06	IGYYRRATRRIRGGD	ORF9 nuc	DR	DR_P01	KDGIIWVATEGALNT	ORF9 nuc	DR
DR_P09	AIVLQLPQGTTLPKG	ORF9 nuc	DR	DR_P02	GTWLTYTGAIKLDDK	ORF9 nuc	DR
DR_P10	YKHWPQIAQFAPSAS	ORF9 nuc	DR	DR_P03	RWYFYYLGTGPEAGL	ORF9 nuc	DR
DR_P16	LSYYKLGASQRVAGD	ORF5 mem	DR	DR_P04	ASWFTALTQHGKEDL	ORF9 nuc	DR
DR_P20	INVFAFPFTIYSLLL	ORF10	DR	DR_P05	ASAFFGMSRIGMEVT	ORF9 nuc	DR
				DR_P07	LLLLDRLNQLESKMS	ORF9 nuc	DR
				DR_P15	FYVYSRVKNLNSSRV	ORF4 env	DR
				DR_P17	IWNLDYIINLIIKNL	ORF6	DR
				DR_P18	QEEVQELYSPIFLIV	ORF7	DR
				DR_P19	SKWYIRVGARKSAPL	ORF8	DR

ID, identification number; spi, spike protein; env, envelope protein; mem, membrane protein; nuc, nucleocapsid protein.

Extended Data Table 4: SARS-CoV-2-specific and cross-reactive HLA class I and HLA-DR T-cell epitope compositions

This table depicts the selection of HLA class I and HLA-DR peptides included in the SARS-CoV-2-specific and cross-reactive HLA class I and HLA-DR T-cell epitope composition (EC) for standardized evaluation in SARS group 2 and PRE group B.

Supplementary Figures, Tables and Data

Supplementary Figure 1: Examples of immunogenic SARS-CoV-2-derived HLA class I-binding T-cell epitopes as evaluated in IFNγ ELISPOT assays. IFNγ ELISPOT assays were performed after 12-day stimulation with the respective SARS-CoV-2-derived HLA class I-binding peptides using PBMCs from convalescent SARS-CoV-2-infected HLA-matched donors. Peptides were analyzed in duplicates. Bars indicate mean spot counts of duplicates normalized to 5 x 10^5 cells with standard deviation. HLA-matched human self-peptides or HIV-derived HLA class I-binding peptides served as negative control. Neg., negative control.

Supplementary Figure 2: Examples of immunogenic SARS-CoV-2-derived HLA-DR T-cell epitopes as evaluated in IFNγ ELISPOT assays. IFNγ ELISPOT assays were performed after 12-day stimulation with the respective SARS-CoV-2-derived HLA-DR-binding peptides using PBMCs from convalescent SARS-CoV-2-infected donors. Peptides were analyzed in duplicates except for SARS019. Bars indicate mean spot counts of duplicates normalized to 5 x 10^5 cells with standard deviation. The Filamin-A-derived peptide ETVITVDTKAAGKGK served as negative control. Neg., negative control.

Supplementary Figure 3: Intensity of T-cell responses against SARS-CoV-2 HLA class I- and HLA-DR-binding peptides as evaluated in IFNγ ELISPOT assays. IFNγ ELISPOT assays were performed after 12-day stimulation with the respective SARS-CoV-2 peptides using PBMCs from convalescent SARS-CoV-2-infected donors. Dots represent individual donors. Bars represent mean with standard deviation.

Supplementary Table 1: Predicted SARS-CoV-2-derived HLA class I peptides selected for immunogenicity screening

This table depicts the sequences, HLA restrictions, peptide positions within the individual ORFs, the prediction scores, and similarity to SARS-CoV-1 of the 100 SARS-CoV-2-derived HLA class I-binding peptides selected for immunogenicity screening.

Supplementary Table 2: Selection of SARS-CoV-2-derived HLA-DR-binding peptide clusters

This table depicts the sequences, HLA restrictions, and peptide positions within the individual ORFs of the HLA-DR peptide clusters selected for immunogenicity screening.

Supplementary Table 3: SARS-CoV-2-derived HLA-DR-binding peptides selected for immunogenicity screening

This table depicts the sequences, HLA restrictions, peptide positions within the individual ORFs, similarity to SARS-CoV-1 and embedded SARS-CoV-2 HLA class I-binding peptide sequences of the HLA-DR-binding peptides selected from the peptide clusters for immunogenicity screening.

Supplementary Table 4: Recurrent mutations of SARS-CoV-2 ORFs within predicted HLA class I peptide sequences

This table depicts recurrent mutations described in the literature within the 100 selected SARS-CoV-2-derived HLA class I-restricted peptides with the wild-type and mutated peptide sequences, reported mutation frequencies, and comparison of SYFPEITHI and NetMHCpan binding scores for the wild-type and mutated peptides, respectively.

Supplementary Table 5: Recurrent mutations of SARS-CoV-2 ORFs within predicted HLA-DR-binding peptide sequences

This table depicts recurrent mutations described in the literature[24,25] within the 20 selected SARS-CoV-2-derived HLA-DR-restricted peptides with the wild-type and mutated peptide sequences and reported mutation frequencies.

Supplementary Table 6: Characteristics of individual SARS donors

This table depicts the individual donor characteristics of all SARS donors (n = 180) with sex, age, HLA type and shows in which group the donors were included.

Supplementary Table 7: Characteristics of individual PRE donors

This table depicts the individual donor characteristics of all PRE donors (n = 185) including sex, age, HLA type and shows in which group the donors were included.

Supplementary Table 8: Immunogenicity screening of SARS-CoV-2-derived HLA class I-binding peptides using IFNγ ELISPOT assays in the SARS and PRE groups

This table depicts the results of the immunogenicity screening of SARS-CoV-2-derived HLA class I-binding peptides with recognition frequencies in HLA-matched donors of the SARS group 1 and PRE group A as well as the assignment of the individual peptides to structural and non-structural or accessory ORFs.

Supplementary Table 9: Alignment of HLA class I SARS-CoV-2 cross-reactive T-cell epitopes to common cold coronavirus sequences

This table depicts the alignment of HLA class I SARS-CoV-2 cross-reactive T-cell epitopes to the sequences of four common cold coronaviruses (HCoV-OC43, HCoV-229E, HCoV-NL63, HCoV-HKU1) with the percentage of identical amino acids, SYFPEITHI score, and NetMHCpan rank.

Supplementary Table 10: Alignment of HLA-DR SARS-CoV-2 cross-reactive T-cell epitopes to common cold coronavirus sequences

This table depicts the alignment of HLA-DR SARS-CoV-2 cross-reactive T-cell epitopes to four common cold human coronavirus sequences (HCoV-OC43, HCoV-229E, HCoV-NL63, HCoV-HKU1) with the percentage of identical amino acids.

Supplementary Table 11: Negative control peptides

This table depicts the negative control peptides used for IFNγ ELISPOT assays, intracellular cytokine and cell surface marker staining.

Supplementary Data 1: Physiochemical properties of SARS-CoV-2 T-cell epitopes in comparison to common cold human coronaviruses

This data set contains physiochemical properties of SARS-CoV-2-derived cross-reactive HLA class I and HLA-DR T-cell epitopes in comparison to four common cold human coronaviruses (HCoV-OC43, HCoV-229E, HCoV-NL63, HCoV-HKU1).